FERROELECTRIC BARIUM STRONTIUM TITANATE THIN-FILM VARACTOR BASED RECONFIGURABLE ANTENNA

Thesis

Submitted to

The School of Engineering of the

UNIVERSITY OF DAYTON

In Partial Fulfillment of the Requirements for

The Degree

Master of Science in Electrical and Computer Engineering

By

Kuan-Chang Pan

Dayton, Ohio

December, 2011

UNIVERSITY of DAYTON

FERROELECTRIC BARIUM STRONTIUM TITANATE THIN-FILM VARACTOR BASED RECONFIGURABLE ANTENNA

Name: Pan, Kuan-Chang

APPROVED BY:

Guru Subramanyam, Ph.D.
Advisory Committee Chairman
Professor/Chair
Electrical and Computer Engineering

Robert P. Penno, Ph.D.
Committee Member
Associate Professor
Electrical and Computer Engineering

Monish R. Chatterjee, Ph.D.
Committee Member
Professor
Electrical and Computer Engineering

John G. Weber, Ph.D.
Associate Dean
School of Engineering

Tony E. Saliba, Ph.D.
Dean, School of Engineering
& Wilke Distinguished Professor

ABSTRACT

FERROELECTRIC BARIUM STRONTIUM TITANATE THIN-FILM VARACTOR BASED RECONFIGURABLE ANTENNA

Name: Pan, Kuan-Chang
University of Dayton

Advisor: Dr. Guru Subramanyam

The main objective of this research is to develop an antenna that can shift its frequency of operation over a band of frequencies. A novel printed antenna for frequency reconfigurable applications is presented. A coplanar waveguide (CPW) antenna was designed on a non-grounded substrate, with the center conductor of the CPW transmission line connected to a bowtie patch. The bowtie structure is the radiating element and lies in the inner space of the annulus created by the CPW ground lines. The antenna has a compact structure with the total area $6 \times 6\ \mathrm{mm}^2$. The frequency of this antenna can be reconfigured from 5.75 GHz to 6.19 GHz by tuning a varactor loaded with the antenna. Applying a DC bias voltage to the ferroelectric (FE) Barium Strontium Titanate (BST) varactor alters the S-parameters of the antenna. The return loss of the antenna in the frequency of operation is below -10 dB, which fits the requirement of a working antenna. The frequency of operation shifts from a lower frequency to a higher

frequency by increasing the DC bias voltage. This reconfigurable antenna was designed, simulated, and fabricated, and the test and measurement results are shown.

ACKNOWLEDGEMENTS

I would like to take this opportunity to express my gratitude to all those who helped me through this research and my years of study at the University of Dayton. My special thanks are in order to Dr. Guru Subramanyam of the University of Dayton, my advisor, for providing the time and equipment necessary for the work contained herein, and for directing this thesis and bringing it to its conclusion with patience and expertise.

I would also like to express my appreciation to Dr. Hai Jiang who introduced and helped me to start my research life in the fields of antenna design. When I first time came to this laboratory, I knew nothing about microwave antennas. Dr. Hai Jiang helped me to learn the antennas, from basic knowledge of what S-parameters are to how the microstrip and coplanar waveguide work differently. He taught me the microwave simulation tool AWR, and helped me to design different types of antennas. I can say, without him, this thesis would not have been possible.

Mark Patterson who is a Ph.D. Student, is also leading this laboratory. Mark helped me to make the masks and processed wafers for the development of the reconfigurable antennas. He is an intelligent person, who always has lots of ideas to create new devices which can be used in practice. I am glad I have this chance to do research with him.

Dustin Brown, a Ph.D. student helped me to complete this thesis. I learnt a lot from him. His serious academic attitude always impresses me and gives me the correct direction while doing research. He is an extremely patient person. When I have questions, he is always willing to help me and spends a lot of time to find the solution with me, and most importantly he never denied helping me even when he was busy. His knowledge always helps me find the best answer and arousing my interest in the field of antenna. I want to express my deep appreciation to him.

I also would like to show my appreciation to Chenhao Zhang who is a master's degree student. He helped me measure all of devices. He is an optimistic person stays upbeat when he gets questions in the research. He really likes to spend his time in the laboratory. Because of him, I began enjoying the research during my studying in UD and enjoy doing research with him. Also, I want to show my appreciation to Hailing Yue and Yi Xu. They always encourage me when I feel down. Also those two ladies are good students. They study really hard, and their behavior encourages me to finish my thesis.

I also want to thank Dr. Gary Thiele who gave me a chance to help him with a typing job for the solution manual of his textbook. I gained a lot of knowledge about antenna during this typing job. Professor Thiele also tried to help me to accomplish my thesis. He gave me two textbooks which are really helpful for me. I really appreciate that he gave me a chance to work for him.

Lastly, I would like to thank my family for their most generous love and support. My parents supported me through all of the expenses and never gave me any pressure. They always say do your best and that made me feel really expressive. I really want to thank my parents for their support and love.

TABLE OF CONTENTS

LIST OF ILLUSTRATIONS

LIST OF TABLES

CHAPTER I

INTRODUCTION

1.1 Motivation

Many types of antennas have been researched, and the characteristics of different antennas can be found in many publications [1]. Different types of antennas have their own specific characteristics, such as being broadband or being highly directive. One common characteristic among most antennas is that they only work over a limited range of frequencies.

Modern communication devices combine many protocols that operate under different frequencies. For example, the working frequencies of a smart phone are between 0.9~2.0 GHz for the global service for mobile communications (GSM), 2.4 GHz for Wi-Fi, 2.4~2.4835 GHz for Bluetooth, and GPS. Therefore, a single limited frequency range antenna cannot satisfy the needs of modern communications. A common method in modern devices to handle the need for transmitting and receiving at different ranges of frequencies is the placement of multiple antennas in one device. As the physical size of a system has an impaction on cost, it is therefore desired to have one antenna that can be used for the multiple frequencies needed for modern communication products.

There are different ways that an antenna can achieve multiple frequency of operation such as a dual-band antenna. Although a dual-band antenna can operate at two different resonant frequencies at the same time, it does not have the characteristic of isolation between bands. Reconfigurable antennas have the feature of shifting their resonant frequency, allowing one specific frequency band at a time. Because of this, the reconfigurable antenna is suitable for modern communications that operate at one band at a time.

Scattering parameters (S-parameters) are used to describe linear electrical networks, and they are obtained by using matched loads to characterize a linear electrical network. The equations of the reflection coefficient are shown in following, as function of incident voltage $\left(V^{+}(x)\right)$ and reflected voltage $\left(V^{-}(x)\right)$ of a transmission line:

$$\Gamma(x) = \frac{V^{-}(x)}{V^{+}(x)} \tag{1.1}$$

Γ is also related to the impedance Z_L

$$\Gamma(x) = \frac{Z_L - Z_o}{Z_L + Z_o} \tag{1.2}$$

where Z_0 is the characteristic impedance of the transmission line:

$$\Gamma(x) = \frac{Y_o - Z_L}{Y_o + Y_L} \tag{1.3}$$

$Y_o = 1/Z_o$ and $Y_L = 1/Z_L$.

The two-port S parameters are defined for the devices that have two ports, and the definitions of it are shown in the following equations:

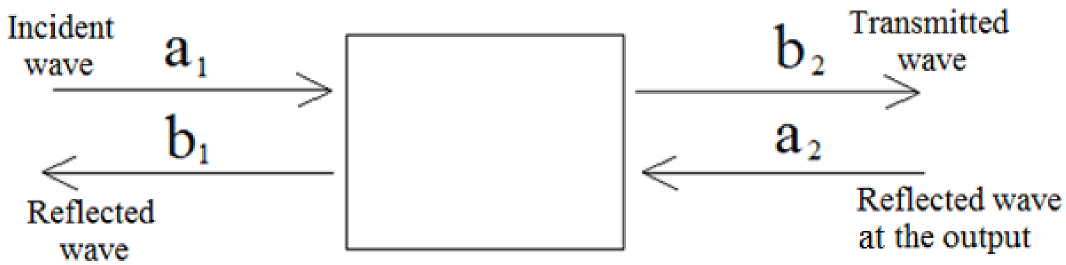

Fig. 1.1: Two-port S parameters

Two port matrix

$$\begin{bmatrix} b_1 \\ b_2 \end{bmatrix} = \begin{bmatrix} S_{11} & S_{12} \\ S_{21} & S_{22} \end{bmatrix} \begin{bmatrix} a_1 \\ a_2 \end{bmatrix} \tag{1.4}$$

$$b_1 = S_{11}a_1 + S_{12} + a_2 \tag{1.5}$$

$$b_2 = S_{21}a_1 + S_{22} + a_2 \tag{1.6}$$

The generalized scattering parameters can then be used to relate the incident and reflected waves, where the i, j^{th} element of a scattering matrix is given by

$$S_{ij} = \left.\frac{b_i}{a_j}\right|_{a_k=0\ for\ k\neq j} \tag{1.7}$$

S_{11} is the input voltage reflection coefficient

$$S_{11} = \left.\frac{b_1}{a_1}\right|_{a_2=0} \tag{1.8}$$

S_{22} is the output reflection coefficient

$$S_{22} = \left.\frac{b_2}{a_2}\right|_{a_1=0} \tag{1.9}$$

S_{21} is the forward voltage gain

$$S_{21} = \left.\frac{b_2}{a_1}\right|_{a_2=0} \tag{1.10}$$

S_{12} is the reverse voltage gain

$$S_{12} = \frac{b_1}{a_2}\bigg|_{a_1=0} \tag{1.11}$$

1.2 Methods of Achieving a Reconfigurable Antenna

Antennas that can alter the radiation pattern or polarization characteristics or the characteristic impedance are generally called reconfigurable antennas [2] [3]. Reconfigurable antennas can be achieved by many technologies such as Microelectromechanical systems (MEMS) switches, materials with tunable microwave/RF properties, and structure modification [1].

Microelectromechanical systems (MEMS) technologies are small electro-mechanical devices ranging from 1 μm ~ 1cm and have been developed for a long time [2]. MEMS have been used in many applications such as varactors, phase shifters, and reconfigurable antennas. These switches have the characteristics of low insertion loss (<1dB), high isolation (>30dB), very low power consumption, good linearity (third order intercept point > 66dBm), and wide frequency bandwidth (dc-40 GHz) [2] [3].

The micromechanical components are fabricated using compatible "micromachining" processes and commonly use silicon as the substrate. MEMS technologies can integrate sensors, actuators, and electronics [3] [4].

MEMS reconfigurable antennas change their bandwidth and resonant frequency by adjusting the length of the antenna physically. A basic MEMS reconfigurable antenna is composed of a thin-metal “bridge” membrane that can be electrostatically actuated to the RF signal line by applying a DC bias [4]. For example, several wire antenna segments can be integrated with MEMS switches in such a way that the MEMS switches can adjust the length of the antenna. The MEMS switches are used to connect desired antenna segments, making a varying frequency and it can also vary the radiation pattern at one frequency [3]. Even though MEMS reconfigurable antennas have many advantages, but RF MEMS switches also have several limitations such a low speed, low power handling capabilities, low mechanical lifetime, high actuation voltage, low reliability, high packaging cost, and fabrication complexity [3].

Ferroelectric (FE) thin-film materials are gaining acceptance in frequency agile electronics and have been applied in many microwave devices because of their nonlinear electric field dependent relative dielectric permittivity (non-linear dielectric tunability) [5]. Ferroelectric thin-film materials are well used in many applications recently, such as electric field-dependent varactors, resonators, filters, phase shifters, voltage control oscillators (VCOs), and reconfigurable antennas [6-12]. Many groups have been researching ferroelectric materials due to their advantages in microwave applications such as small size, light weight, high switching speed, low power consumption, high integration capability, and low actuation voltage [2]. Barium Strontium Titanate ($Ba_{(1-x)}Sr_xTiO_3$) (BST) has been applied in ferroelectric tunable microwave circuits [5], is one of the most popular ferroelectric thin-film materials currently being studied for room temperature microwave applications [5].

Some important characteristics of BST thin-films are large field dependent permittivity, high dielectric constant ($\varepsilon_r > 500$), and low loss tangent ($\tan\delta = 0.02$). This material overcomes some of the disadvantages of $SrTiO_3$ (STO) thin-films, such as low tunability (<20%) and poor performance at room temperature for microwave applications. Another characteristic of thin-film BST is that the film has a higher dielectric constant and loss tangent at lower electric field, but the dielectric constant and the loss tangent reduce with higher electric field concentration [2]. The measured results of the relative dielectric constant and loss tangent with a bias voltage applied across the thin-film are shown in [2].

Ferroelectric reconfigurable antennas work by changing the characteristic impedance of the antenna by altering the dielectric properties of the ferroelectric by the application of different electric fields.

1.3 Comparison of the MEMS Reconfigurable Antennas and Ferroelectric Reconfigurable Antennas

From the previous section it is known that reconfigurable antennas have good uses in microwave systems and recent theoretical and experimental research results have demonstrated applications using MEMS and ferroelectric materials.

First, it is known that the size of the devices is important in microwave applications, because of the relationship to cost. Ferroelectric BST thin-films have the characteristic of high dielectric constant, and the higher dielectric constant can reduce the size of microwave antennas [13] [14]. The BTFV reconfigurable antenna can achieve the miniaturized antenna and save more space than MEMS reconfigurable antennas by using FE BST thin-films. Second, the cost to manufacture the ferroelectric reconfigurable antenna should be lower than MEMS reconfigurable antenna because there are no mechanical devices in the ferroelectric reconfigurable antenna, which can lead to significant manufacturing savings. Third, MEMS antennas are subject to device fatigue limiting the product lifetime in certain applications. The ferroelectric reconfigurable antenna does not have such fatigue concerns [2] [3]. In addition, MEMS reconfigurable antennas are subject to coupling between sections. Because MEMS reconfigurable antennas use switches to connect or disconnect two pieces of metal, when these metals are close enough, they have a coupling effect even when the switch is off. Table 1.1 summarizes the comparison between MEMS reconfigurable antennas and ferroelectric reconfigurable antennas.

Table 1.1 Performance comparison between MEMS and ferroelectric reconfigurable antennas
[2] [3]

	MEMS Reconfigurable antenna	Ferroelectric Reconfigurable antenna
Size	Average	Small
Radiation/Gain	Average	Low
Cost-manufacture	High	Low
Fatigue	Yes	No
Actuation voltage	High (30V)	Low (~10V)

1.4 Research Questions to be Addressed

The thin-film varactor has been demonstrated as a phase shifter, and has been integrated with a microstrip patch antenna. However, the use of a CPW antenna integrated with a varactor has not been researched. For the reconfigurable antenna, there are several design difficulties.

1. Can a CPW varactor be implemented with a CPW antenna for reconfigurability of the antenna?

There are different shapes of CPW antennas. Examples are patch antenna, spiral antenna, and bowtie patch antenna. The antennas needed to be researched and simulated to find if they can shift their frequency of operation.

2. Can an antenna be designed to operate and shift at a specific frequency?

It is ideal that the frequency will shift to a desired frequency when a properly biased varactor is integrated with the antenna, but the range of operating frequencies an antenna can tune to is unknown. The range of tunable frequencies for antenna/varactor combinations will need to be determined.

3. Is the voltage needed to shift the frequency in a reasonable range?

The optimum frequency range of the CPW antenna is adjusted through the DC bias voltage. However, it is desired to have the frequency shift over low voltage, 0 ~ 10 V. It is unknown what voltage will provide the necessary shift to cover the needed frequencies.

The research questions will be discussed in following chapters. In Chapter 2, some basic concepts of the BST thin-film varactor will be introduced. The CPW fed bowtie slot antenna will be discussed in Chapter 3, and the simulated and measured results of the reconfigurable antenna will be shown in Chapter 4.

CHAPTER II

LITERATURE REVIEW

2.1 Literature Review of Ferroelectric BST Thin Films and Applications

Ferroelectric $Ba_xSr_{1-x}TiO_3$ (BST) thin-films have been well developed and used in the past decades. BST thin-films are getting important due to their characteristics of high dielectric constant, low dielectric loss, and large tunability with different doping levels [15] [16]. The dielectric constant of ferroelectric BST thin-films can be tuned by adding external DC bias voltage. Therefore, many researchers are involved in research on ferroelectric BST thin-films, and the characteristics of the FE BST thin-films are used in microwave devices can have high integration capability, high switching speed, small size, light weight, low power consumption, and low actuation voltage [2]. FE BST thin-films are attractive microwave devices such as phase shifter, filters, and varactors. FE BST thin-film materials have a characteristic temperature which is called the Curie temperatureT_C, at which the material can make a structural phase change from a polar phase (ferroelectric) to a nonpolar phase (paraelectric) [17]. The ferroelectric phase possesses an equilibrium spontaneous polarization that can be reoriented by an applied electric field (i.e., hysteresis loop). At the non-polar (paraelectric) phase, the relative dielectric constant (ϵ_r) still remains large, and the ferroelectric possesses zero spontaneous polarization that can be changed by the applied electric field. This characteristic enables the fabrication of electronically tunable capacitors with large tunabilities (> 50%) at dc-bias in 2–5 V [2] [17]. This kind of capacitors is often used in tunable microwave devices. Tunability and loss tangent are the parameters of a dielectric material that quantifies its inherent dissipation of electromagnetic energy. BST has higher tunability and it is suitable for integration in system operating at room temperature [16].

2.2 Varactors

Ferroelectric thin-films can be used in many microwave applications. Interdigital electrodes and parallel-plate electrodes are one of those ferroelectric BST thin-film applications, and they are used to measure dielectric properties at different frequencies. The interdigital capacitor (IDC) is often used in surface acoustic wave devices, while the parallel-plate capacitor (PPC) is appropriate for ferroelectric tunable capacitors [15]. The structure of coplanar interdigital capacitor (IDC) has several metal parts interchanged with each other and looks like fingers. The signal spreads to the multiple metal parts using fringe capacitance created between adjacent fingers from either side of the signal port as shown in Fig. 2.1. Because the IDC is one layer structure and do not have high overlapping effective area, they can handle higher operating voltage [16]. Another type of the varactor is parallel-plate capacitor (PPC). The structure of the PPC will be discussed in the next chapter, FE BST thin-film varactor.

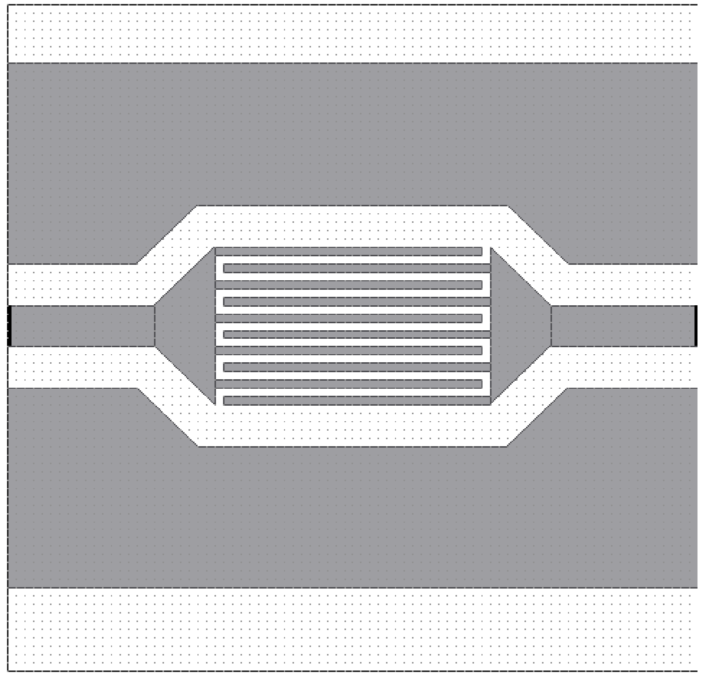

Fig. 2.1: The structure of the interdigital capacitor (IDC)

2.3 Filter

Microwave filters have been used in different types of communication systems such as receiver preselection, intermediate frequency (IF), and transmit filtering [17]. There are several types of tunable filters. For example, microelectromechanical systems (MEMS) and ferroelectric thin films have been wide used in tunable filters. MEMS filters have some advantages like low insertion loss which is approximately 4 dB, and can handle high voltage like hundred volts. However, MEMS based filters have several disadvantages. The tuning speed of it is around microsecond, and the cost of packing is high. Compared to MEMS based filter, the ferroelectric BST thin-film based filter have low cost, high tuning speed around a few nanosecond, low dielectric loss, and high tuning capacity at room temperature [17-20].

2.4 Phase Shifter

Phase shifters are used to change the transmission phase ($\angle S_{21}$) in a network, and BST thin-film can also be used in a phase shifter to provide variable phase shift and better resolution. Ferroelectric BST thin-film phase shifter can have the advantages of low insertion loss, high power handling, instantaneous phase change response, and approximately equal loss in all phase states. For a tunable phase shifter a 50 ohm system, low loss and large phase shift are expected. Most phase shifters are reciprocal networks, and the output of a phase shifter is directly proportional to the electrical length in the phase shifter hence related to the square root of the effective permittivity. Ferroelectric BST thin-film phase shifters are electrically controlled phase shifters. The phase of electrically controlled phase shifters can be varied by DC voltage [16] [19].

CHAPTER III

FE BST THIN-FILM VARACTOR

3.1 Coplanar Waveguide (CPW)

Coplanar waveguide transmission line consists of three metal lines above a dielectric substrate, and operates as either coplanar stripline or slotline. The CPW transmission line in Fig. 3.1 is a coplanar stripline as it consists of a signal line and two ground planes. The characteristic impedance of the CPW transmission line is controlled by the signal line width, s, and the two gaps, w_1 and w_2 seen in Fig. 3.1. Typically $w_1 = w_2$ in CPW lines.

The structure of coplanar stripline CPW is the mode utilized hereafter, and will be the type referred to when mentioning CPW. The type of CPW utilized does not use a ground plane on the bottom layer. One advantage of this CPW structure is better dispersion characteristics than microstrip. Additionally, as the three ends (which are signal and two grounds) exist in one plane, no via is needed to ground the transmission line. Because of this, the CPW has lower loss when dealing with shunt elements than microstrip.

Because devices using this type of transmission line lie on the top of the dielectric, there may be coupling problems in the packaging of CPW structures. These effects may lead to additional losses at high frequencies. This problem can be solved by adding some ground planes around the transmission line to increase electrical isolation and avoiding noise [21].

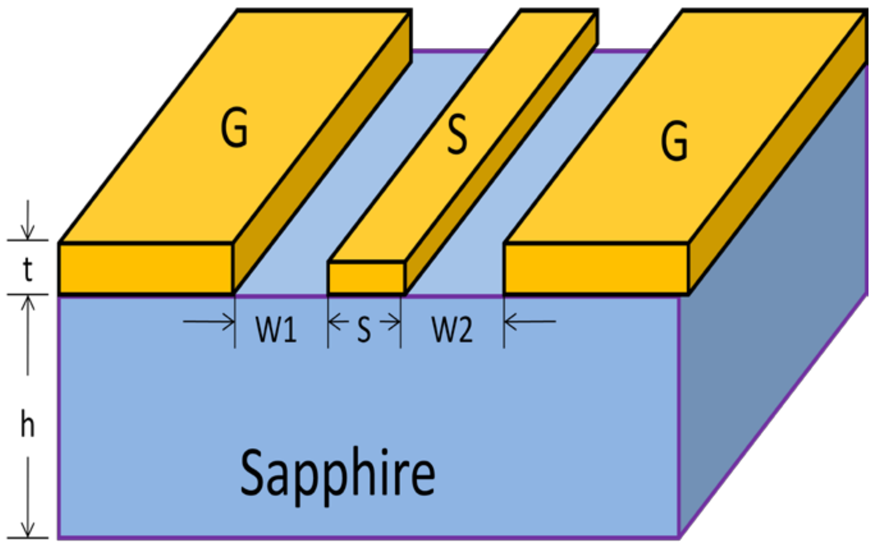

Fig. 3.1: The basic structure of coplanar waveguide

3.2 BST Thin-Film Varactor

The ferroelectric BST thin-film varactor (FBTV) is an important device for the reconfigurable antenna. The varactor to be used is a ferroelectric thin-film based shunt switch device and has two ports. It can be used for microwave and millimeterwave switching applications. The ferroelectric varactor is a two metal layer structure based on a coplanar waveguide transmission line [22-25]. The top metal layer is a CPW structure which consists of ground, signal, and ground lines. The bottom metal layer looks like an English alphabet "H" which consists of two ground lines and a shunt line between the two ground lines. The two ground lines in the bottom metal layers have the same dimension as the grounds in the top layer which can be seen in Fig. 3.2.

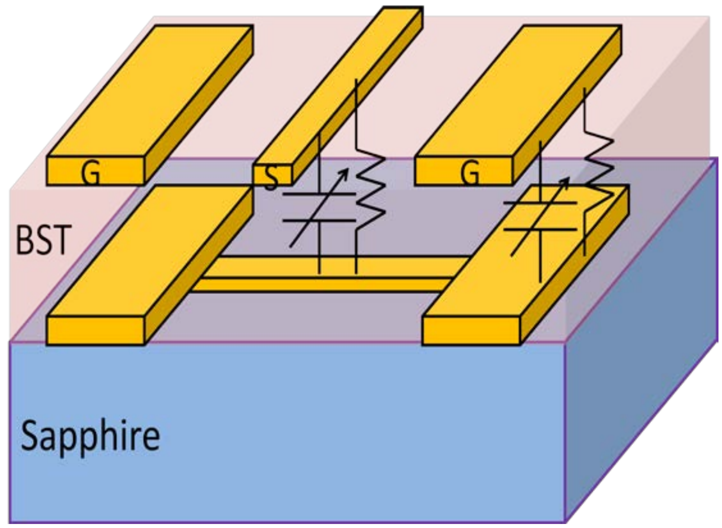

Fig. 3.2: The structure of the varactor-based capacitive shunt switch

0.25 μm thick BST material lies between the two metal layers. Sapphire is used as the substrate with a thickness of 600 μm (Fig. 3.3). The dimensions of the BST thin-film varactor from the top view is $500 \times 450\mu m^2$. The width of the signal line is $50\mu m$, while the width of the ground line is $150\mu m$, and the distance between the ground plane and signal line is $50\mu m$ (Fig. 3.4).

Because the thickness of the BST is only ~$0.25\mu m$, there is a maximum external DC bias that can be placed between the top and bottom metal layers without creating a short circuit. The maximum external DC bias is therefore set to approximately 10 V. As the DC bias is applied, the BST thin-film between the conductors adjusts the phase velocity of the transmission line, behaving as a tunable capacitor.

Fig. 3.3: The layers of the varactor-based capacitive shunt switch

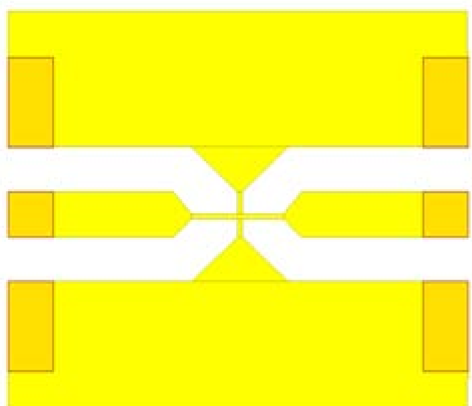

Fig. 3.4: The top view of the varactor-based capacitive shunt switch

The capacitance of the varactor *C(V)* is shown in equation 3.1

$$C(V) = \frac{\varepsilon_o \varepsilon_r(\mathrm{V})\ \mathrm{A}}{d} \tag{3.1}$$

where A is the area of overlap between the signal line and shunt line, d is the thickness of the BST layer, V is the DC bias, and C is the capacitance of the BST thin-film varactor.

ε_o is the permittivity in free space, $\varepsilon_r(V)$ is the voltage dependent permittivity of the BST thin-film. From equation 3.1, it shows the relation between capacitance, dielectric constant and the dimension of the varactor. When the dimension is big, the capacitance will be large. The high capacitance will cause power loss and short the circuit. The Fig 3.4 shows the electrical model of the varactor. To avoid the short circuit, the overlap area of the varactor was made smaller, and the capacitance will be smaller as well.

Because a suddenly tapered 90° would increase transmission line losses, the transmission line of the varactor is tapered 45° in the overlap area. The two edges of the varactor are designed as 50 Ohms CPW transmission line (Fig.3.5). The measurement results of scattering parameters (S parameters) S_{11} and S_{21} of the varactor in different DC voltage are shown in Fig. 3.6. This figure shows the S_{11} and S_{21} in voltage 0V and 10 V.

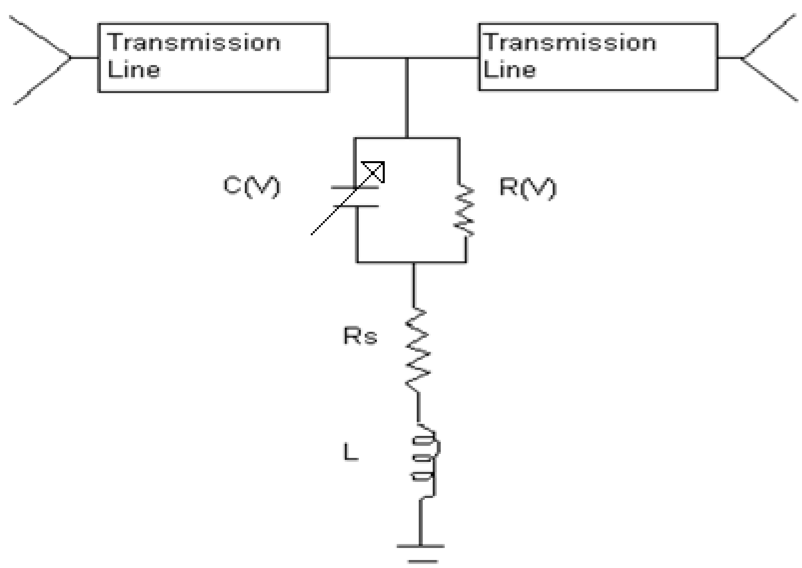

Fig. 3.5: The electrical model of the varactor-based capacitive shunt switch [24]

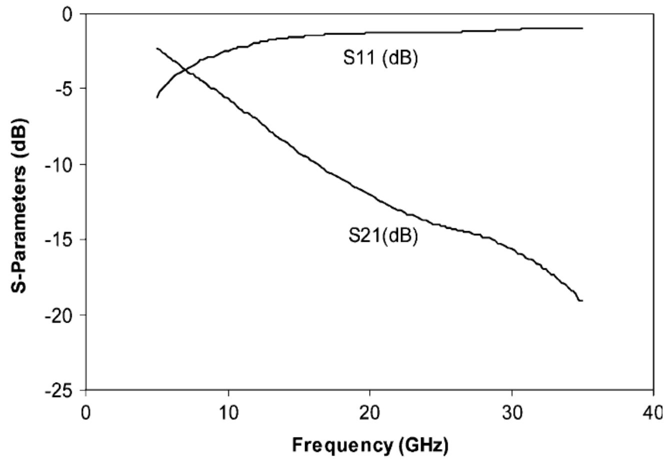

(a)

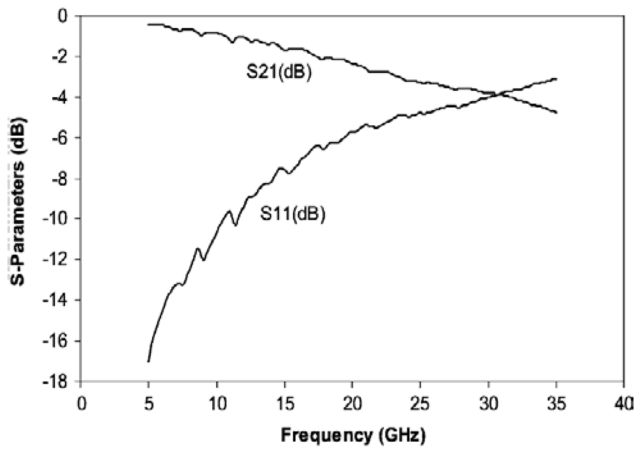

(b)

Fig. 3.6: The varactor shunt switch at an applied bias of (a) 0 V and (b) 10 V [24].

The value of the inductance is derived in equation 3.2.

$$L = \frac{Z_0}{2\pi f} \sin\left(\frac{2\pi f}{\lambda_g}\right) \tag{3.2}$$

The f is the operation frequency of the varactor, and the λ_g is the guide wavelength of the transmission line. Z_o is the characteristic impedance of the transmission line.

The shunt resistance in the electrical model of the varactor is shown in equation 3.3

$$R_d = \frac{1}{\omega C(V) \tan \delta} \tag{3.3}$$

ω in the equation 3.3 is the operating angular frequency, and the $\tan \delta$ is the loss tangent of the BST thin-films. The $\tan \delta$ is derived as follows.

$$\tan \delta = \frac{\varepsilon''}{\varepsilon'} \tag{3.4}$$

$$\varepsilon = \varepsilon' - j\varepsilon'' \tag{3.5}$$

In the equation 3.5, the dielectric constant ε is complex quantity, and it includes a real part and as imaginary part. The real part shows the relative dielectric constant of ε_r and the imaginary part expresses the information about the shunt conductance of the ferroelectric materials of the BST thin-films [2].

CHAPTER IV

CPW FED BOWTIE PATCH ANTENNA

4.1 Introduction

Microwave antennas have been developed for a long time, and they have been applied in many areas, especially mobile phones. Microwave antennas have different characteristics, such as broadband, high gain, or high quality factor. The examples of narrow band microwave antennas are microstrip, and coplanar waveguide (CPW) fed antenna.

There are different shapes of antennas, such as patch antennas, spiral antennas, and bowtie patch antennas. Each of these antennas has their own advantages. For this reconfigurable antenna, a wide bandwidth is desired, so a bowtie antenna is a good choice, because the antenna acts similar to a dipole antenna but with wider bandwidth. As the name implies, a bowtie patch antenna resembles a bowtie shape. This antenna has two conical planar sections combined together, and the two triangular planes can be metal or dielectric. The bowtie antenna is fed in the center section where the two triangular planes are connected.

There are different ways to feed the bowtie antenna (coplanar waveguide, microstrip line, and parallel strip line), and the choice of feeding line can affect the input impedance to the antenna. Microstrip line is the most common transmission line to feedthis antenna, but the coplanar waveguide is just as easy to use as a feed to the bowtie antenna.

Printed CPW fed antenna have several advantages over microstrip patch antennas.Compared to microstrip patch antennas, CPW antennas have better impedance matching when integrated with the varactor because it is based on a CPW transmission line [26]. Also, a CPW antenna has several advantages, such as low dispersion, easy integration with active devices, and it has the ability to effectively control the characteristic impedance [27] [28]. CPW fed antennas are simple to fabricate by using modern printed-circuit technology [24]. They also have the characteristic of broadband, and low radiation loss [27-36].

The input impedance can be matched with quarter wavelength transformers, $Z = \sqrt{Z_o Z_L}$. For an antenna, the reflections and ringing effects often happen at the feed points, and the way to reduce those effects is to load the antenna [1].

In this CPW fed bowtie patch antenna, sapphire is used as the substrate. The dielectric constant $\varepsilon_r$of sapphire is 9.7, and thickness is 600 µm. There is no ground plane on the bottom of the CPW bowtie antenna. The substrate has an important effect for designing a miniaturized antenna because its higher dielectric constant can help reducing the size of antenna [13] [14]. The substrate material is sapphire in this research. The Barium-Strontium-Titanate (BST) thin-film is deposited on the top of the sapphire substrate. The reason that the antenna is been put on two layers, which are sapphire and BST, is the varactor needs to be integrated with the antenna. The antenna and the varactor are integrated together, and the antenna is on the top of the two layers for which the lower layer is Sapphire and the upper layer is BST. The dielectric constant ε_r of the BST is characterized as 600 at 0 V [37] [38], and its thickness is 0.25 μm. ϵ_r of BST of 1000 at 0 V has been measured in our lab.

4.2 Simulation of the Reconfigurable Antenna

The commercial microwave frequency simulation tool, AWR is used to simulate the S-Parameters of possible antenna structures. AWR is a powerful piece of software for simulating microwave devices including microwave antennas. Because AWR was used to simulate the BST thin-film varactor, there was a benefit to using the same software for the antenna as well.

AWR has two 3D-planar EM Simulators EMSight & Axiem both are based on Method of Moments (MOM) solvers. Method of Moments is often used to solve linear partial differential equations. The advantages of Method of Moments are fast solutions because it is only calculating boundary values rather than values throughout the space. It is also efficient with problems with a small surface to volume ratio. However, the disadvantages of this method are that the results are not very accurate because Method of Moments only estimates the outside of the parameter space. Another disadvantage is that it might take more time to do the calculation according to the problem size.

The first step was to create an electromagnetic (EM) structure. This process involves defining the enclosure size, material definitions, and dielectric layer definitions. The size of grid needs to be chosen as this affects how many solution points the software has to find. The smaller the size of the grid, the more accurate the results should be. However, decreasing the grid size will increase the simulation time as well. The shape of the antenna can be created after the size of the grid is set. Once the simulation is complete, AWR can provide results of antenna resonant frequencies and radiation patterns.

There were two antennas that have been designed. The size of the first antenna is$8 \times 8\ mm^2$, and the size of the second is $6 \times 6\ mm^2$. The varactor is$0.5 \times 0.45\ mm^2$. Compared with the varactor, the bowtie patch antenna is much bigger. Because of this the size of the grid used by AWR was needed to be set to a larger size. The simulation time depends on the value of the dielectric constant, the size of the devices, and the size of the grid.

It is known that what affects the simulation time, but how to keep the accurate simulation results when the simulation time is reduced. First, the higher dielectric constant value can make the simulation time longer in AWR. In this experiment, the value of ε_r of BST was tried to be reduced, so the simulation time can be made faster, however, if the value of ε_r of BST was changed, the capacitance could not be kept the same, and the simulation results would not be accurate. The way that keeps the same capacitance when ε_r of BST is changed is the width of the transmission line of the varactor needs to be changed as well. When the dielectric constant of BST becomes smaller, the width of the transmission line of the varactor needs to become wider. Therefore, the capacitance of the varactor is still the same. The relationship between dielectric constant of the BST and capacitance of the varactor can be seen in equation 3.1, $C(V) = \frac{\varepsilon_0 \varepsilon_\mathrm{r}(\mathrm{V})\ \mathrm{A}}{d}$.

4.3 Ideal Antenna Sizing

For an antenna to be useful, the return loss $|S_{11}|$ should be below -10dB. This bowtie antenna is CPW structure, and there is no ground plane on the bottom of the antenna. In the beginning, the antenna is assumed to be put in free space, and size of the space which is the enclosure is sat as 15000 μm for x axis and 12000 μm for y axis.

The electric field is around the bowtie patch, but it is not strong in the ground plane. The Fig. 4.1 shows the E field of the CPW bowtie patch antenna, and the color yellow area indicates the stronger E field in the antenna.

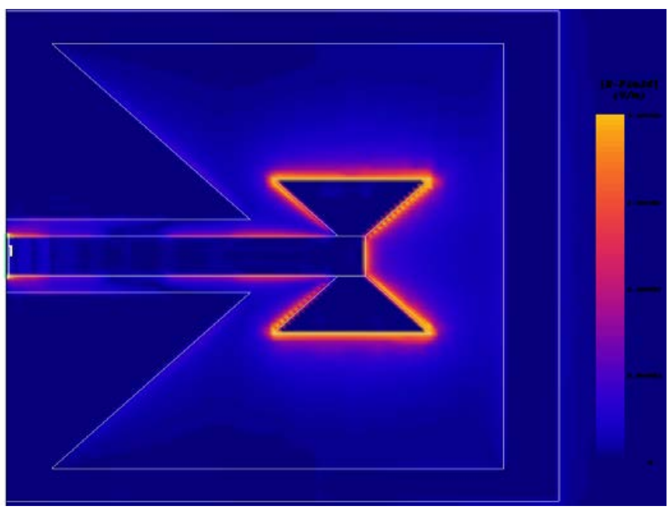

Fig. 4.1: Planar EM simulation of the antenna for E field

Because there is a perfect conductor around the bowtie shape patch, the size of the enclosure does not need to be large based on the observation that most of the electric fields are just around the bowtie patch and not on the outside of the CPW structure. Therefore, the currents will not be affected by a small enclosure. This should make simulation times faster, without affecting the results.

The structure of the antenna is different with FE BST thin-film varactor (FBTV). The varactor is a two ports device, and it needs to contact with the two boundaries for adding edge ports. However, the antenna is a one port device, and it only needs to contact with a boundary for adding edge port as shown in Fig. 4.2 and 4.3.

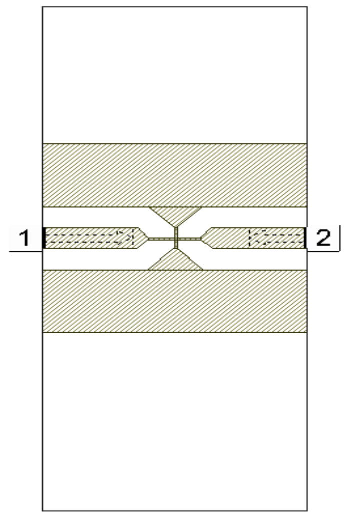

Fig. 4.2: FE BST thin-film varactor in AWR

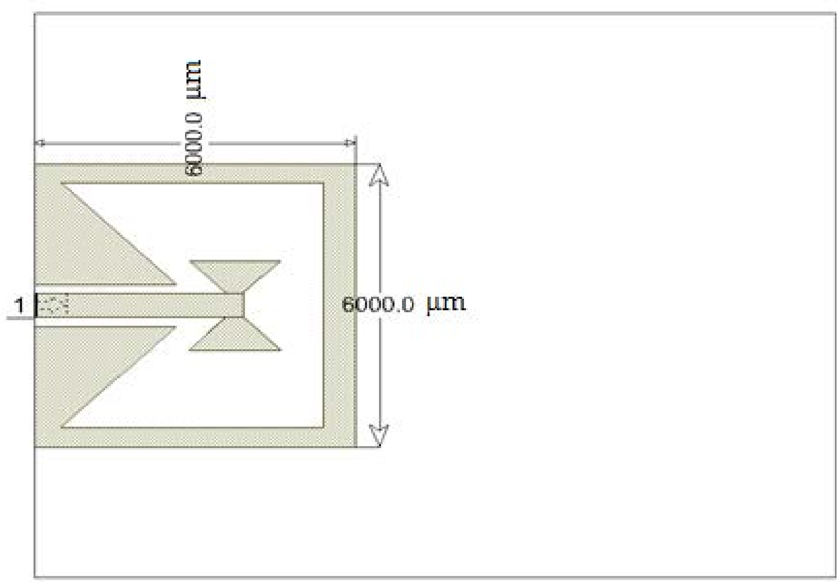

Fig. 4.3: CPW fed bowtie patch antenna in AWR

The size of the grid is 50 μm for simulating the antenna. The default of the AWR places a perfect electric conductor (PEC) on the top and bottom of the enclosure. However, there is no ground on the bottom layer and top layer on CPW antennas. The bottom and top layers were set as open. For using AWR, the size of free space boundary can have the effect for the antennas. Some errors may be caused when the size of the boundary is not set properly.

4.4 The Optimized or Best Resulting Antenna

The Fig. 4.4, 4.5 and table 4.1, 4.2 show the dimensions and sizes of the CPW bowtie patch antennas. The simulated resonant frequency of the miniaturized CPW bowtie antenna 1 is 7.71 GHz. The sizes of the bowtie structure patch are $L = 4.8\ mm$ and $W = 5.1mm$ which is approximately $0.12\ \lambda_o \times 0.1275\lambda_o$. The width of the transmission line is set as 500 μm, and the gap between the transmission line and ground plane is set as 200 μm.

The operating frequency of the second CPW bowtie antenna is 5.8943 GHz. The sizes of the bowtie structure patch are $L = 1.65\ mm$ and $W = 1.9\ mm$ which is approximately $0.0324\ \lambda_o \times 0.0373\ \lambda_o$. The width of the transmission line is set as 500 μm, and the gap between the transmission line and ground plane is set as 200 μm.

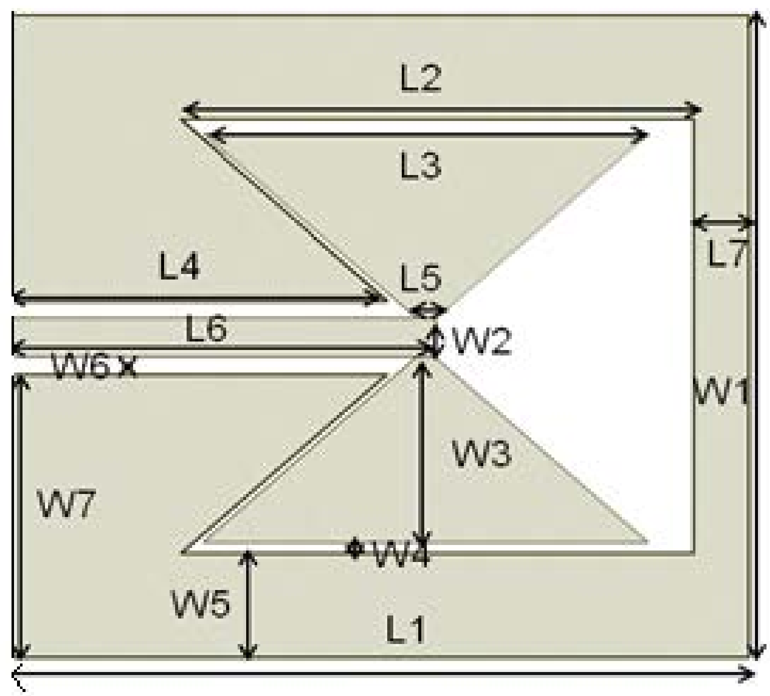

Fig. 4.4: The structure of the CPW bowtie patch antenna 1

Table 4.1 The geometry of CPW bowtie antenna 1

Wide	mm	Length	mm
W1	8	L1	8
W2	0.5	L2	5.55
W3	2.3	L3	4.8
W4	0.15	L4	4.1
W5	1.3	L5	0.2
W6	0.2	L6	4.6
W7	3.55	L7	0.6

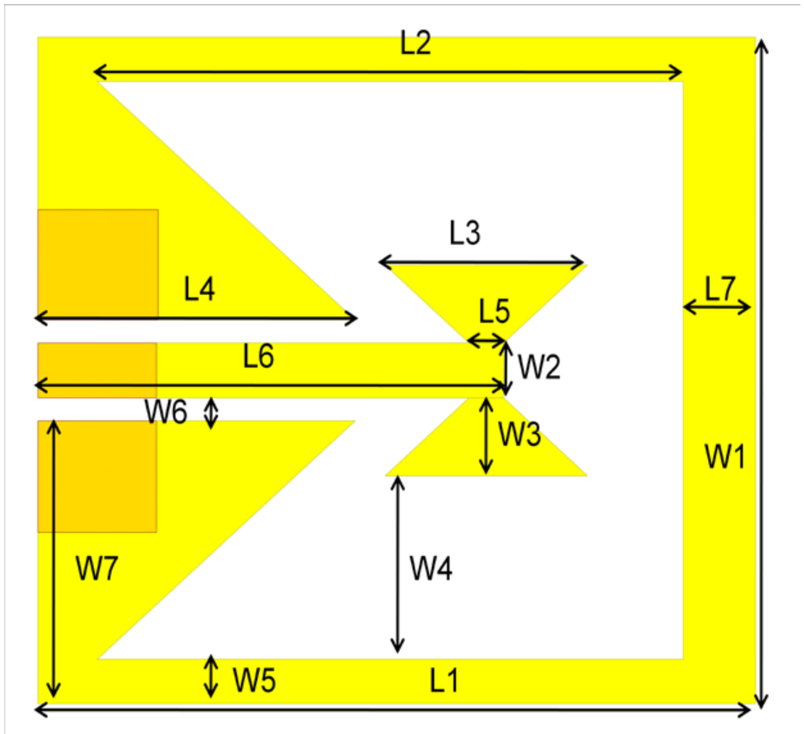

Fig. 4.5: The structure of the CPW bowtie patch antenna 2

Table 4.2 The geometry of CPW bowtie antenna 2

Wide	mm	Length	mm
W1	6	L1	6
W2	0.5	L2	4.9
W3	0.7	L3	1.65
W4	1.65	L4	2.65
W5	0.4	L5	0.3
W6	0.2	L6	3.9
W7	2.55	L7	0.6

Compared to conventional CPW bowtie antennas; those antennas are twenty times smaller because the substrate with a high permittivity is used in this design [13] [14]. The antennas are matched to the CPW line with characteristic impedance of 50 ohms. The simulated resonant frequency of the CPW bowtie antenna 1 is shown in Fig. 4.6. The resonant frequency of the simulation result for the antenna 1 is 7.71 GHz and the return loss is 29.73 dB for the first antenna. The resonant frequency of the simulation result for the second antenna is 5.89 GHz, and the return loss is -43.83dB. The resonant frequency of the measured result is 5.83 GHz, and S_{11} is -11.86 dB. The resonant frequencies of the simulated and measured results are really close, but the reflection coefficients differ. The reason for this may be the dielectric constant of the BST in the fabricated antenna was different with the simulated value. Also, the modeling assumes a low dielectric constant material as the superstrate, where as in actual devices, the high dielectric constant is the superstrate resulting in low bandwidth of the antenna and higher return loss.

An approximate formula [39], for the characteristic impedance of the coplanar waveguide,

$$Z_o = \frac{30\pi^2}{\sqrt{(\varepsilon_r + 1)/2}}\left[\ln\left(2\,\frac{1+\sqrt{k}}{1-\sqrt{k}}\right)\right]^{-1} \tag{4.1}$$

$$k = \frac{w}{w + 2s} \tag{4.2}$$

w = center transmission line width, and s = the slot width between the transmission line and ground. $w = 500\ \mu m, s = 200\ \mu m$, the $Z_o = 48.89$ is around 50 Ohms. ε_r = relative dielectric constant of the dielectric substrate. The substrate is sapphire, and its dielectric constant $\varepsilon_r = 9.7$. The concept of aperture reconfiguration can be extended to include control of radiation pattern through changing the receiving/transmitting elements of the antenna in near real time.

The Fig.4.7 shows the simulated results of Smith chart of the CPW bowtie antenna 1 and 2. The simulated and measured resonant frequency and Smith charts of CPW bowtie antenna 2 are shown in Fig. 4.8 and Fig. 4.9. When the CPW bowtie antenna was fabricated, the antenna was loaded with FE BST thin-film varactor, so there is no measured Smith chart for bowtie antenna1. The Fig 4.7 shows there is phase shift between the simulated antenna 1 and 2, and Fig. 4.9 shows the phase shift between simulated and measured result for the CPW bowtie patch antenna 2. The phase shift also could be due to the high dielectric constant superstrate resulting in a higher effective dielectric constant hence lower guide wavelength compared to the theoretical simulation results.

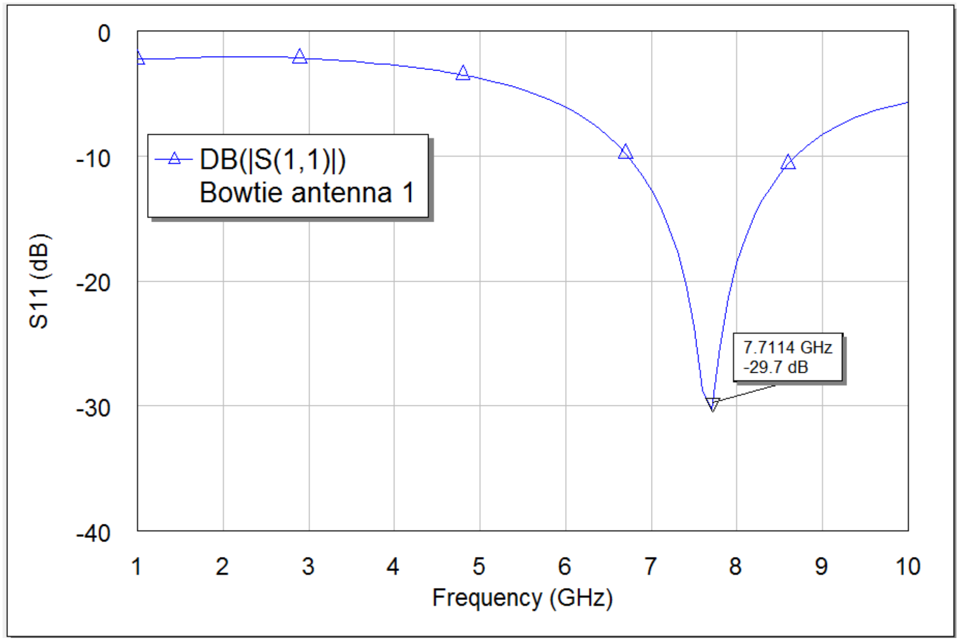

Fig. 4.6: The simulated resonant frequency of CPW bowtie antenna 1

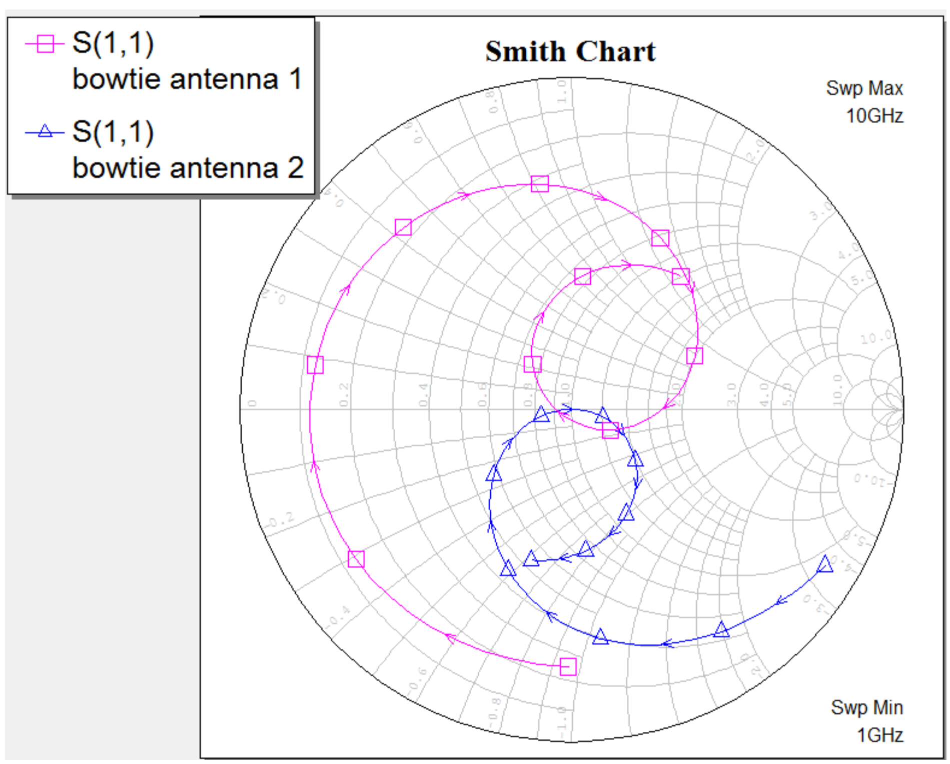

Fig. 4.7: The simulated Smith chart of CPW bowtie antenna 1 and 2

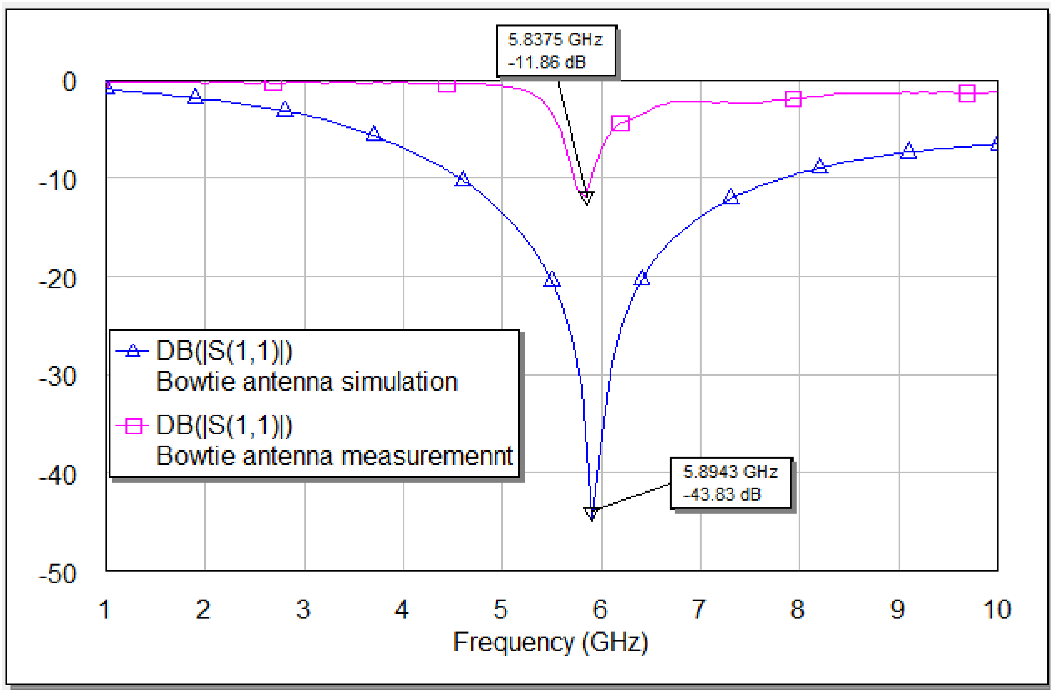

Fig. 4.8: The simulated and measured resonant frequency of CPW bowtie antenna 2

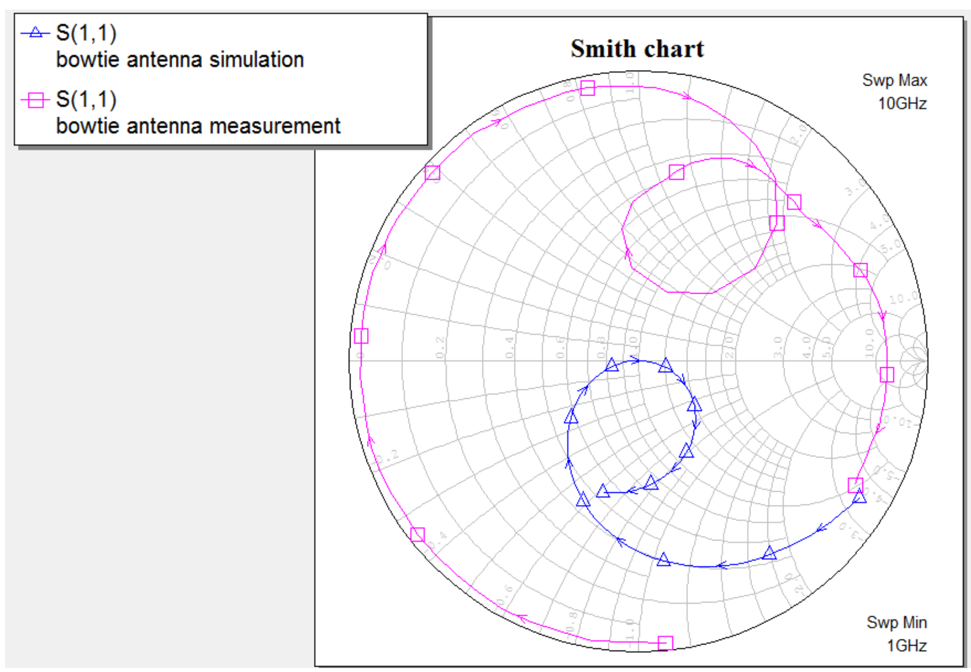

Fig. 4.9: The simulated and measured Smith chart of CPW bowtie antenna 2

CHAPTER V

RECONFIGURABLE ANTENNA

5.1 Introduction

In this CPW bowtie antenna, the inclusion of an integrated varactor [30] shifts the initial resonant frequency of the antenna to a lower point, and the resonant frequency can be shifted to a higher frequency with increasing DC bias. The advantage is that the size of the antenna can be made smaller and still having the characteristic of low frequency. The varactor is loaded in front of the transmission line of the CPW bowtie antenna [29]. The type of the antenna in [29] is a microstrip patch antenna. Compare to the microstrip patch, there are several advantages to use CPW fed bowtie patch antenna. First, it can simplify the fabrication. The structure of varactor is CPW. When the varactor is placed with microstrip patch antenna, the transmission line needs to be converted from CPW to microstrip. Second, it is easier to get the impedance matching when the varactor is integrated with CPW antenna. Furthermore, CPW bowtie antenna does not need extra DC bias for the circuit network if the varactor is integrated in front of the bowtie antenna. The DC bias can be directly added to the varactor. Even the size of the bowtie patch antenna can be changed and make its frequency lower, but the goal of this research is to design the reconfigurable antenna, so the operating frequency of the antenna is set as 5.89 GHz, and try to reconfigure the frequency.

A FE BST thin-film varactor (FBTV) integrated with an antenna has been presented in [29]. The type of the antenna in [29] is a microstrip patch antenna. The varactor was integrated in front of the feed line of the microstrip patch antenna, and the figure of it is shown in [29]. The result was simulated, but the antenna was not fabricated. Although the antenna was not fabricated, the results of the simulation show the frequency is shifted to a lower frequency when compared to the antenna without a varactor. The frequency shifts back to higher range when a DC bias voltage is added from 0V ~ 10 V.

The tuning frequency of the reconfigurable antenna 2 is expected to be in 3 GHz. To achieve this range of frequency, the multiple thin-film varactors were added for increasing the range of frequency tuning. The size of the bowtie antenna 2 is $6 \times 6mm^2$, and its resonant frequency is 5.89 GHz.

5.2 Electromagnetic Simulation

Next step, the frequency tuning of the reconfigurable antennas will be simulated. To simulate the frequency tuning of the reconfigurable antennas, another function which is circuit schematic in the AWR was used to simulate if the frequency can be tuned. Circuit schematic is the function which can simulate different devices and combine them together. For example, the CPW bowtie patch antenna and BST thin-film varactor were simulated separately, so the simulation time for each of them is fast. However, if the two devices were put together without changing the size of the varactor, the AWR could not simulate it due to inadequate memory. To solve this problem, the function of the circuit schematic was used, and it can make the CPW bowtie patch antenna and BST thin-film varactor as two electrical models and connected together as shown in Fig. 5.1. The big advantage of this function is the device can be simulated by itself, and the memory will not be inadequate.

In chapter 3, the characteristic of the BST was introduced. The dielectric constant of the BST is varied with the DC bias voltage. When the DC bias is changed from 0 ~10 V, the dielectric constant of the BST will be decreased. For simulating the resonant frequencies of the reconfigurable antenna in DC bias from 0 V to 10 V, the dielectric constant of the BST was changed as well.

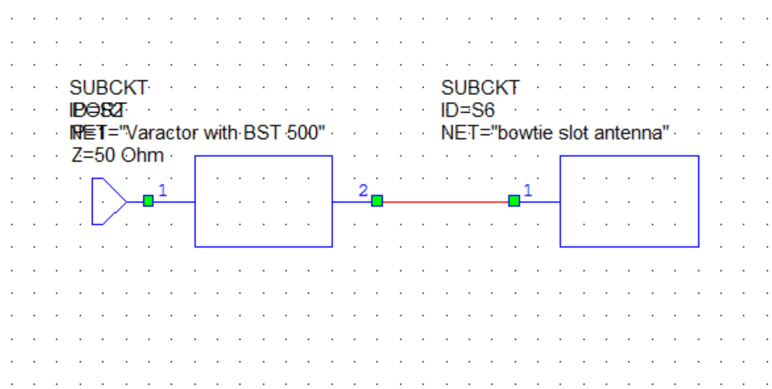

Fig. 5.1: Circuit schematic to simulate the reconfigurable antenna

Based on the simulation results, the resonant frequency of the antenna 2 is 5.89 GHz. The return loss of CPW bowtie antenna 2 is -43.83dB. The bandwidth of the CPW bowtie antenna 2 is 55.6%. The higher voltage is added, the lower ε_r will be [2].

$$f = \frac{1}{2\pi\sqrt{LC}} \tag{5.1}$$

Furthermore, the equation can show the relations between voltage and frequency. It has been demonstrated that the ε_r decreases when DC voltage increases, and capacitance decreases when ε_r decreases in $C(V) = \frac{\varepsilon_0 \varepsilon_r(V)\, A}{d}$. The resonant frequency increases when capacitance decreases. Therefore, the resonant frequency increases when DC bias voltage increases.

The Fig. 5.2 and 5.3 show the simulation results of a varactor integrated with the CPW bowtie antennas 1 and 2, and those antennas are named reconfigurable antenna 1 and 2. The results of the reconfigurable antenna 1 are not good enough because the resonant frequencies are not shifted regularly. Some of them shift to lower point and they are supported to be in higher frequency range when the DC bias is increased. The table 5.1 shows the data of the simulated results of the reconfigurable antenna 1.

From the results of reconfigurable antenna 2, the resonant frequency shifts to lower range and shifts to higher range when adding DC bias voltage. When DC bias voltage changes, the dielectric constant will change as well. Therefore, the different values of the dielectric constant are used to simulate the added DC bias voltage. The simulation results for the dielectric constant from 500 to 30 are shown. The data of the simulation for the reconfigurable antenna 2 can be seen in Table 5.2.

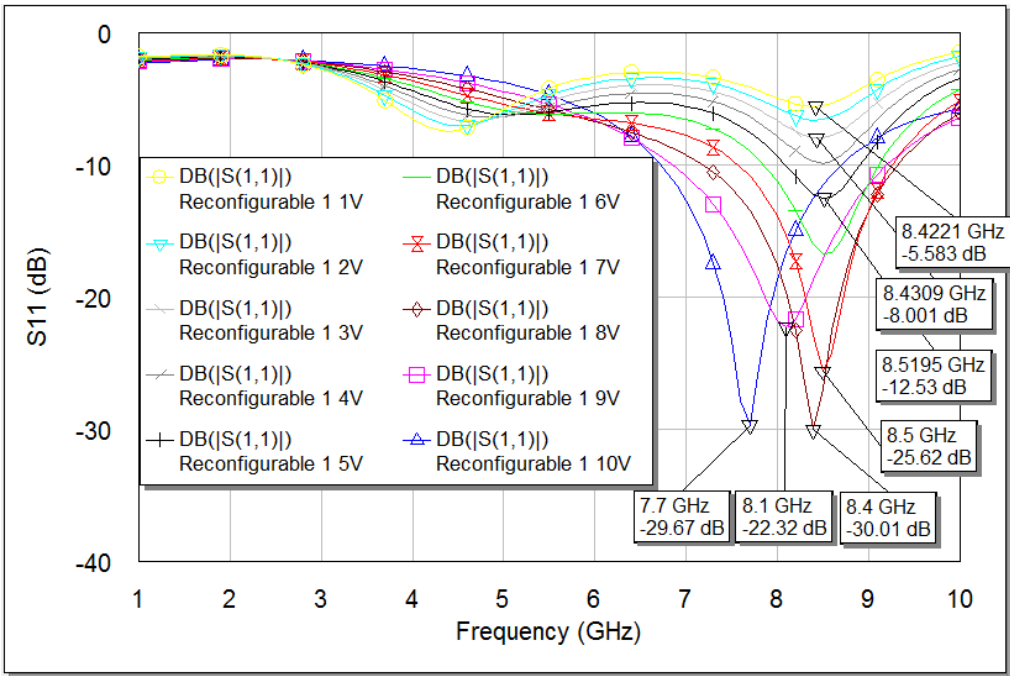

Fig. 5.2: Using circuit schematic to get simulation results of reconfigurable antenna 1

Table 5.1 The data for the simulation results of reconfigurable antenna 2

Voltage (V)	Dielectric constant εr	Frequency (GHz)	S11 (dB)
1	500	8.4221	-5.583
2	450	8.4945	-6.609
3	400	8.4309	-8.001
4	350	8.5098	-9.877
5	300	8.5195	-12.53
6	250	8.5578	-16.68
7	200	8.5	- 25.62
8	150	8.4	-30.01
9	100	8.1	-22.32
10	30	7.7	-29.67

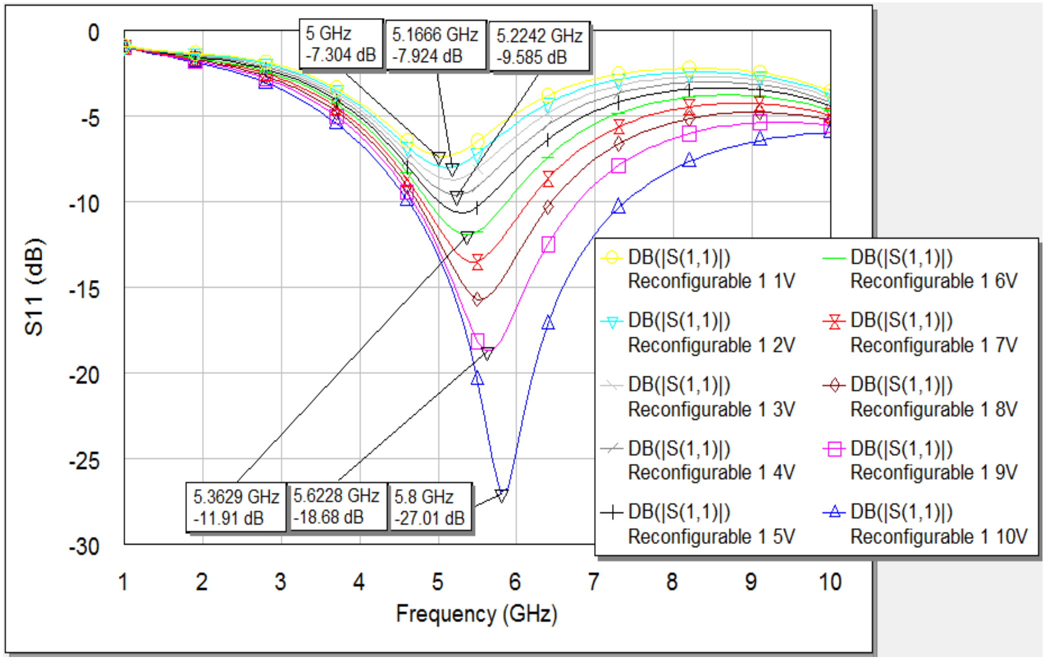

Fig. 5.3: Using circuit schematic to get simulation results of reconfigurable antenna 2

Table 5.2 The data for the simulation results of reconfigurable antenna 2

Voltage (V)	**Dielectric constant εr**	**Frequency (GHz)**	**S11 (dB)**
1	500	5.000	-7.304
2	450	5.1666	-7.924
3	400	5.1864	-8.695
4	350	5.2242	-9.585
5	300	5.3124	-10.64
6	250	5.3629	-11.91
7	200	5.500	- 13.5
8	150	5.5323	-15.67
9	100	5.6228	-18.68
10	30	5.800	-27.01

5.3 Process of the Fabrication

Once a successful design was simulated, the AWR structure was put in a mask for fabrication. The mask was used in the creation of fabricated sapphire wafers containing the reconfigurable antenna. The wafers were fabricated at clean rooms at Wright

Patterson Air Force Base and the University of Dayton.

The first step in the fabrication process was the placement of the bottom metal of the varactor using standard positive photoresist lithography [40] [41]. The bottom metal is made of Titanium (Ti) (20 *nm*) / platinum (Pt) (100 *nm*)/ gold (Au) ($1\mu m$) / Pt (100 nm). The wafer was then coated with a 0.25 μm thick $Ba_{0.6}Sr_{0.4}Ti_{03}$ (BST) thin-film. A Neocera Pioneer 180 pulsed laser deposition (PLD) system (Neocera, Beltsville, MD) was used to deposit the BST thin film [2]. The top metal is Ti (20 *nm*) / Pt (100 *nm*)/ Au ($1\mu m$) and was created in a process identical to that for the bottom metal, using positive photoresist lithography.

5.4 Results of the Fabricated Antenna

Once the fabrication was complete, the antenna was measured in the KL411 lab at the University of Dayton. A network analyzer and an on-wafer microwave probe station were used to measure the S parameters, gain and frequencies of the reconfigurable antenna. There is one varactor loaded with the CPW antenna 1, and the measured results are shown in Fig. 5.4 and table 5.3. For tuning/reconfiguring the resonant frequency, three varactors are integrated with the CPW bowtie antenna 2. The reconfigurable antenna which used three varactors in front of the CPW bowtie antenna showed no resonance or tuning when first testing the antenna. Therefore, the probe was placed between the second and third varactor (shown in Fig. 5.5). The measurement skips the first two varactors. As the probe is located between in second and third varactor, the optimum frequency can be measured, and it is shifted to 5.75 GHz in DC bias voltage 0V and shifted to higher range 6.19 GHz when the voltage is 10 V. The measured results are shown in Fig. 5.6 and Table 5.4. The photos of the reconfigurable antenna 2 are shown in Fig. 5.7.

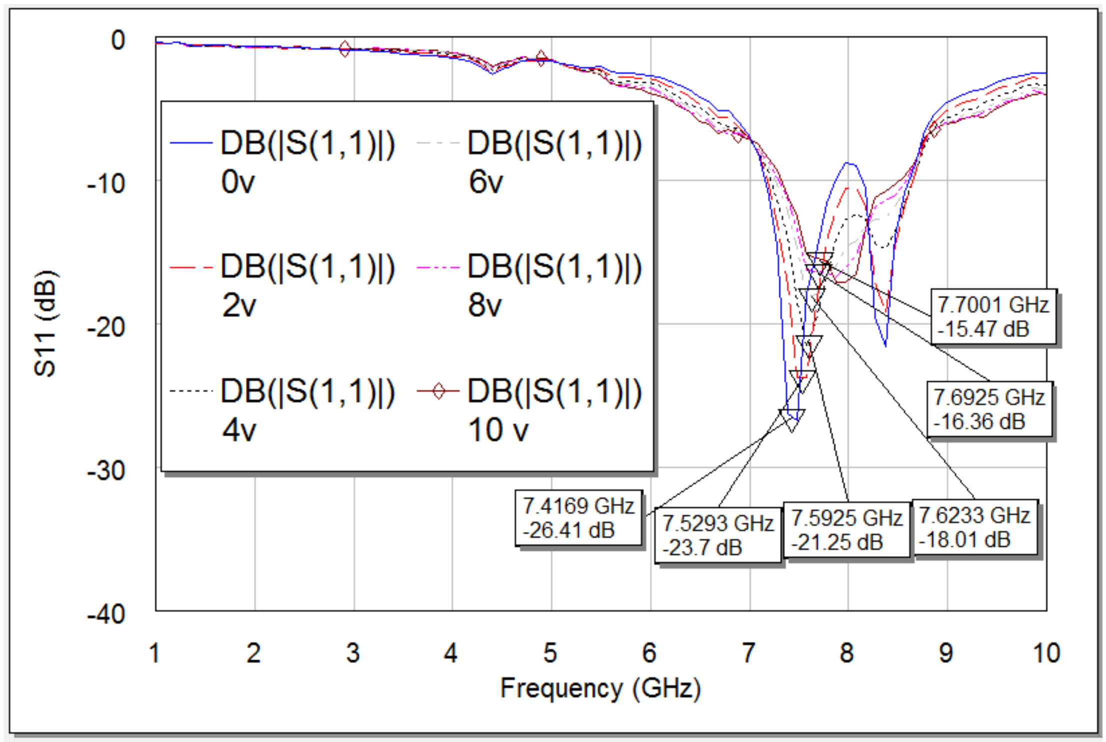

Fig. 5.4: The measurement results of the reconfigurable antenna 1

Table 5.3 The measured results of the reconfigurable antenna 1 for the frequency range at different DC voltages

Voltage (V)	**Frequency (GHz)**	**S11 (dB)**
0	7.4169	-26.41
2	7.5293	-23.7
4	7.5925	-21.25
6	7.6233	-18.01
8	7.6925	-16.36
10	7.7001	-15.47

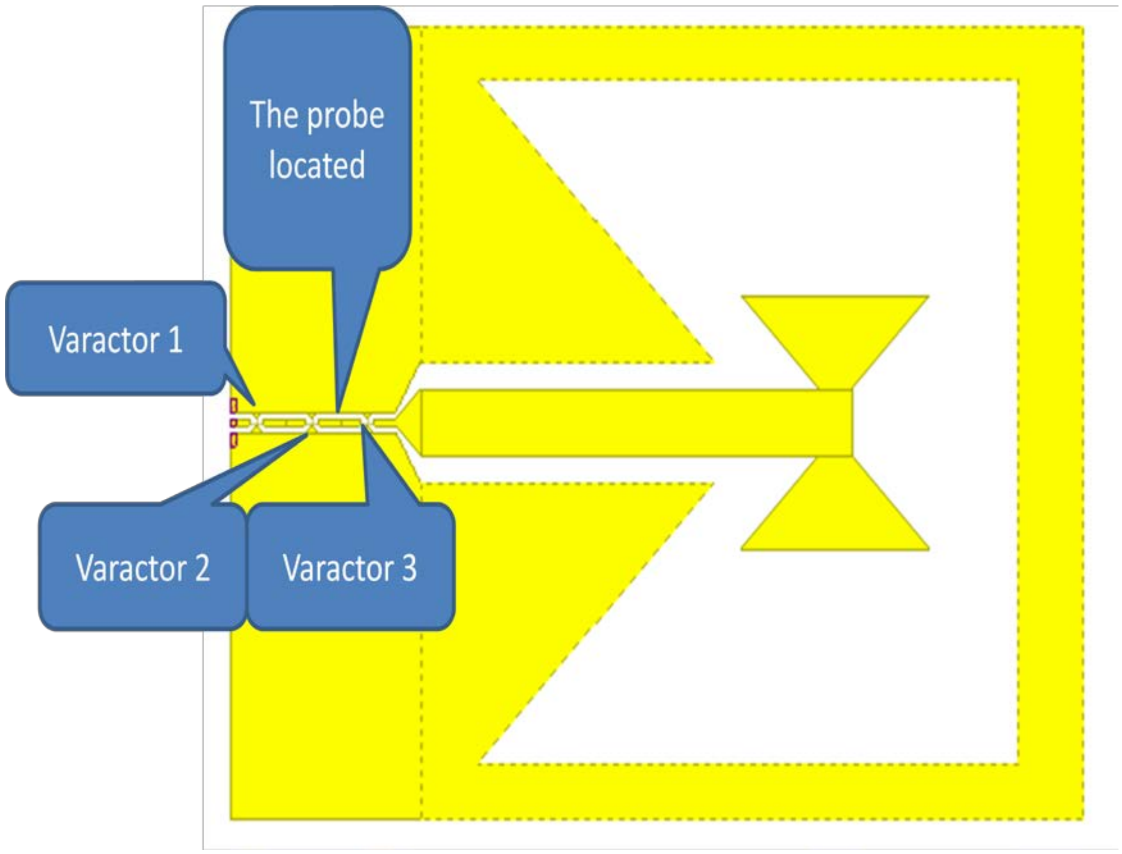

Fig. 5.5: The shape of reconfigurable antenna 2 (Three varactors integrated with the CPW bowtie antenna 2)

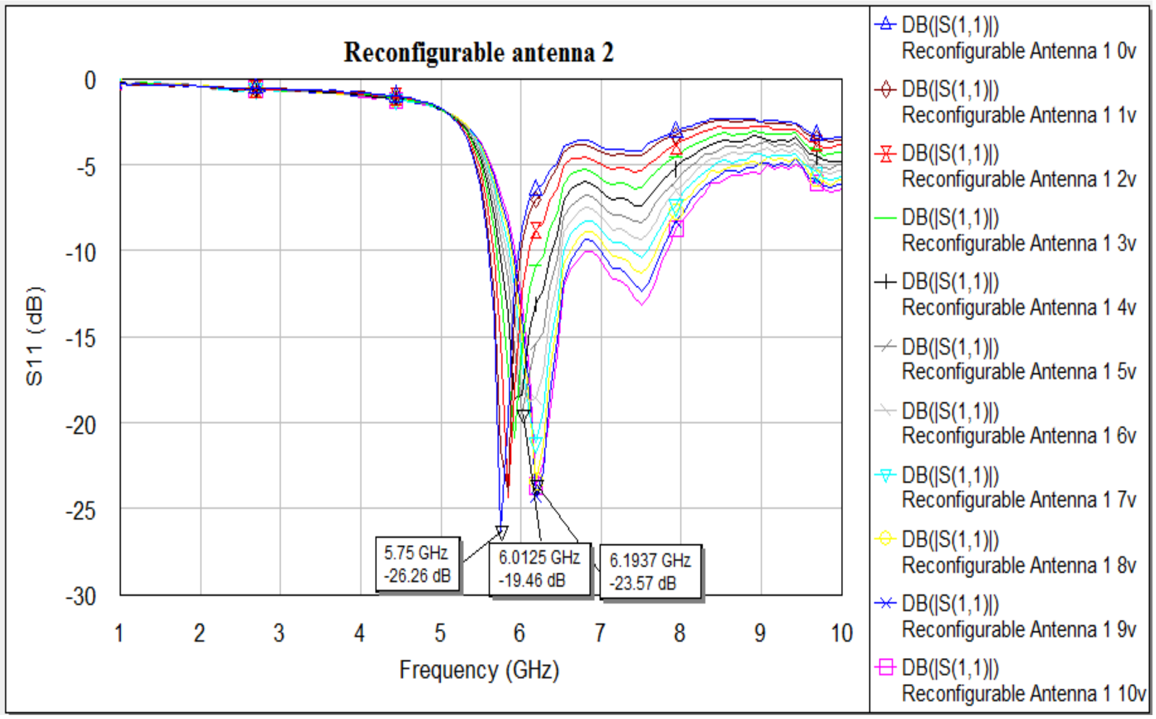

Fig. 5.6: The measurement results of the reconfigurable antenna 2

Table 5.4 The measured results of the reconfigurable antenna 2 for the frequency range at different DC voltages

Voltage (V)	**Frequency (GHz)**	**S11 (dB)**
0	5.75	-26.26
1	5.7698	-22.18
2	5.8375	-24.39
3	5.9167	-20.55
4	5.9859	-18.45
5	6.0125	-19.46
6	6.1261	-18.7
7	6.1845	-21.09
8	6.1875	-23.42
9	6.1914	-24.22
10	6.1937	-23.57

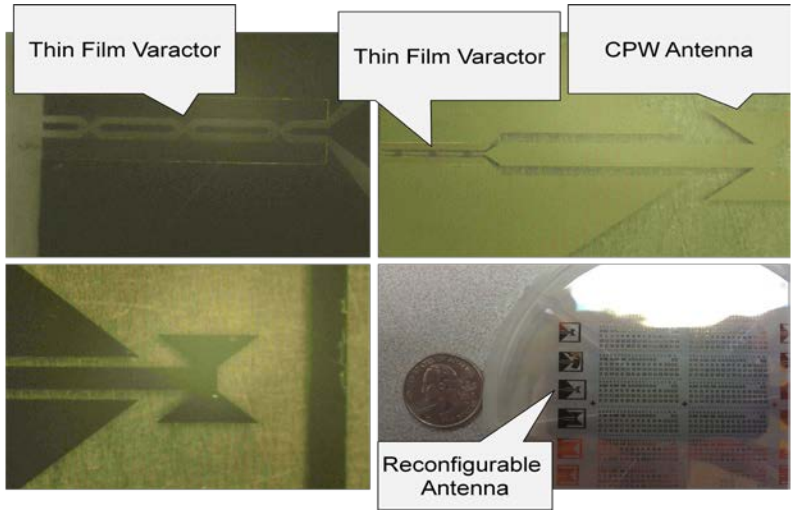

Fig. 5.7: The photos of the fabricated reconfigurable antenna 2

The far field radiation patterns of the reconfigurable antenna were measured at Radiation and Scattering Compact Antenna Laboratory (RASCAL) in the Air Force Research Laboratory. To measure the far field radiation patterns, the reconfigurable antenna was turned mechanically in an anechoic chamber. A rotating mast was in the center of the chamber, with a portable probe station connected to it. The probe station was used to hold the antenna as shown in Fig. 5.8. The antenna acted like a receiver and the signal traveled through the probe station's cable where the magnitude and phase data was collected and measured. For each mechanical sweep, both co-polarized and cross-polarized fields were used. The process was repeated for the other cut. The results of the co-polarized E plane, cross-polarized E plane, co-polarized H plane, and cross-polarized H plane were calibrated by comparing patterns from a calibration antenna. After these steps, the data shown is calibrated gain, and the radiation patterns of the reconfigurable antenna 1 were shown in Fig. 5.9 and 5.10. For the results of radiation patterns, only the reconfigurable antenna 1 has been measured, the reconfigurable antenna 2 could not be included in this thesis.

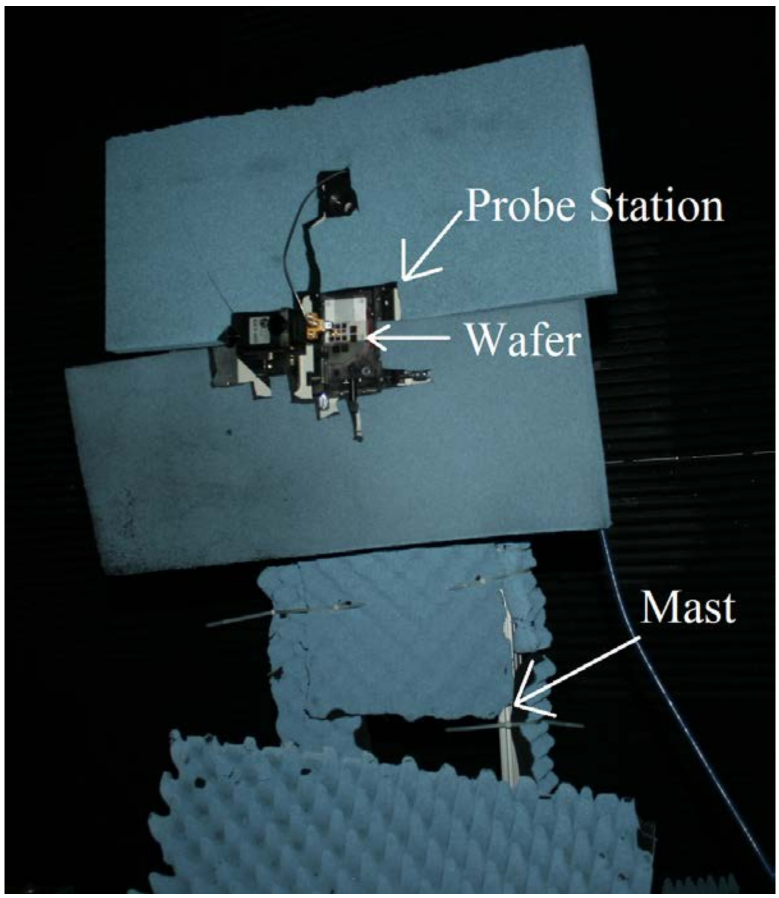

Fig. 5.8: An anechoic chamber at RASCAL in the Air Force Research Laboratory

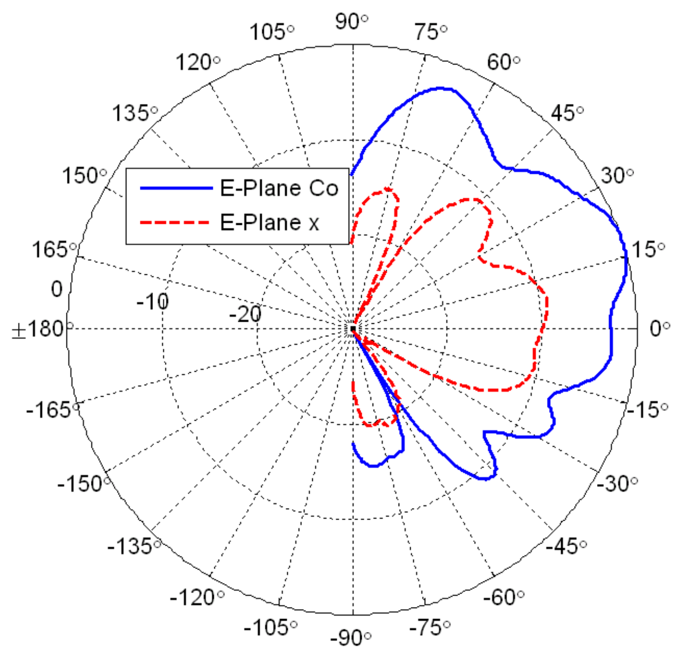

Fig. 5.9: E-plane Co-polarization and Cross-polarization measured at the frequency of 7.3 GHz for the reconfigurable antenna 1

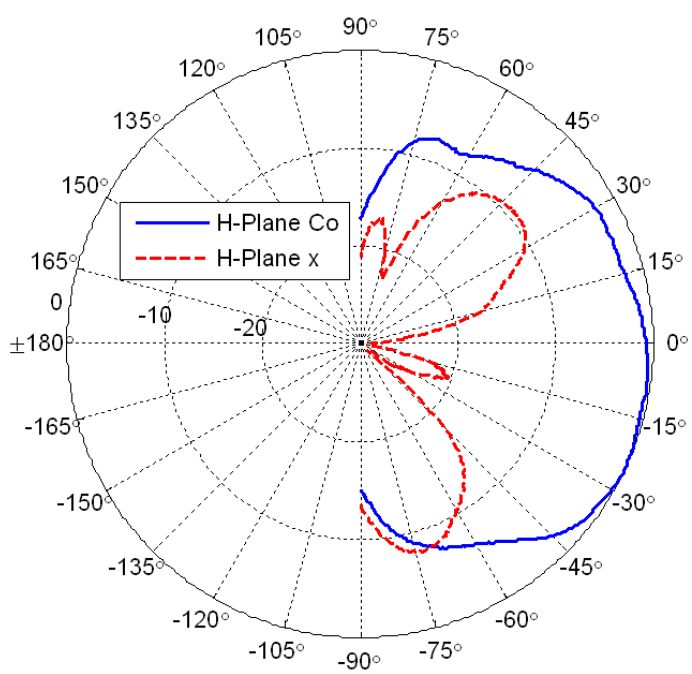

Fig. 5.10: H-plane Co-polarization and Cross-polarization measured at the frequency of 7.3 GHz for the reconfigurable antenna 1

According to the CPW fed bowtie patch antenna. The ground plane is moved from the bottom layer to the same layer as the patch located, and there is no ground plane below the substrate. When the wafer was tested, the platform of the microprobe test station was used to hold the antenna, and it is made of metal. When the antenna was laid on the platform, the platform acted like a ground plane. To avoid the conductor effect of the return loss from the platform, the part of the wafer where reconfigurable antenna was fabricated was moved to the outside of the platform, and the reconfigurable antenna was tested outside the platform. The rest part of the wafer still stayed on the platform and held by the vacuum on the wafer chuck platform. Compared to simulation results, the measurement results of the resonant frequencies are higher, but the return loss of the measurement results is better than simulation results. The reason for this might be that the dielectric constant of the fabricated reconfigurable antenna is different than the simulated one, or the fabricated reconfigure antenna has three varactors with it, and the simulated reconfigurable antenna has one only varactor with it. Even the two varactors of the fabricated reconfigurable antenna are skipped; they might have some effects with the results.

The analyzer that was used to measure these values was HP 8720B network analyzer and the probe used was CASCADE SP-ACP40-GSG-150-C. The desired DC bias voltage is applied to the signal lead of the probe using a bias tee. To calibrate the equipment to make sure accurate results, a Line-Reflect-Reflect-Match calibration wafer was used. Then, the S parameters are recorded and saved for a range of DC biases from 0-10V. The DC supply was used in this laboratory is Keithley 2400 source meter, and the bias tee was Picosecond Model 5531. The DC voltage was send to the probe through the DC bias tee and cable.

The second reconfigurable antenna was designed because the simulated and measured results of the reconfigurable antenna 1 are not good enough. There is a notch in the reconfigurable antenna 1, and this notch might be caused by the FE BST thin-film varactor, also the size of the second CPW bowtie antenna is smaller than the first one, and the operating frequency of the second antenna is lower than the first antenna. For the reconfigurable antenna 2, the frequency shifted range of the simulation results is around 0.8 GHz. The S_{11} of the simulation results is -7.3dB in 1 V, and it is -27 dB when the DC voltage is 10 V. Compared to the simulation results, the experimental frequency shift is around 0.5 GHz which is lower than the simulation results, but the S_{11} of the measurement results is around -20 dB which is better than the simulation results. The comparison of the results for the simulation and measurement in 1V and 10 V are shown in Fig. 5.11.

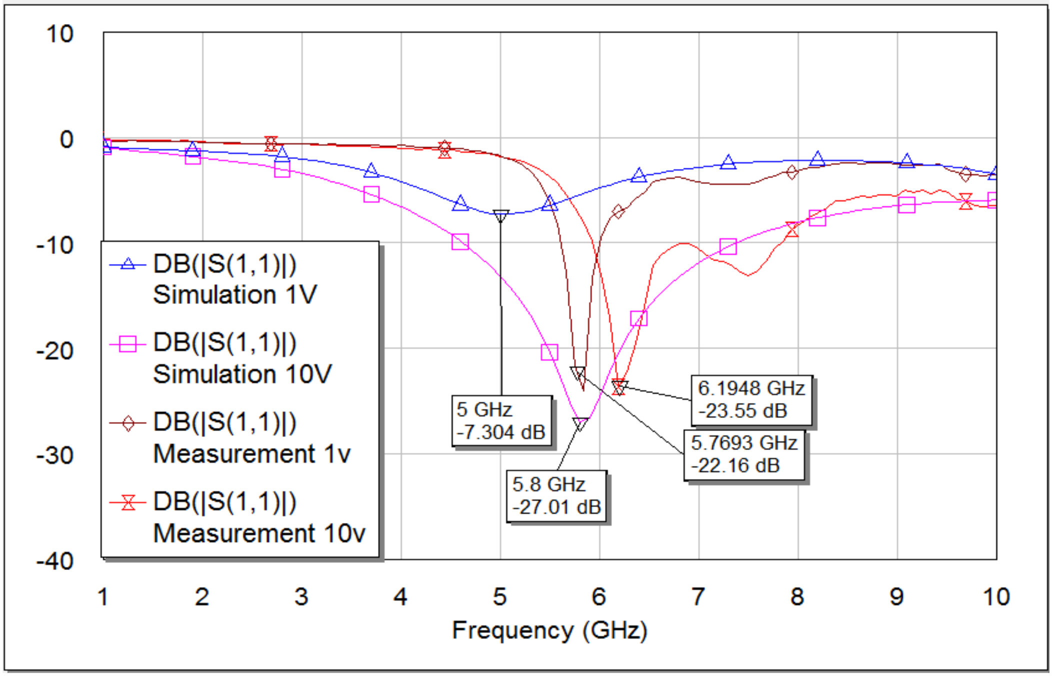

Fig. 5.11: Reconfigurable antenna 2 comparison of simulated and measured

It has been discussed about the advantages and disadvantages of the MEMS and FBTV reconfigurable antennas. The two are compared in this section. A MEMS reconfigurable antenna in paper [42] is been compared with this FBTV reconfigurable antenna because both of these antennas use DC bias voltage to control the capacitance, and then shift the resonant frequency. The shifted range of the MEMS reconfigurable antenna is around 0.49 GHz in lower frequency range which is 9.87 GHz at 0V and 9.48 GHz at 30 V. In the upper frequency range, the shifted range is around 0.88GHz, and the resonance frequency is 12 GHz at 0V and 11.12 GHz at 30 V.

The shifted range of the FBTV reconfigurable antenna is around 0.45 GHz which is from 5.75 GHz in 0 V to 6.19 GHz at 10 V. The shifted range of the FBTV reconfigurable antenna is smaller than the MEMS reconfigurable antenna, however, the range of the DC bias for the MEMS reconfigurable antenna is from 0 V to 30 V, and the range of the DC bias for the FBTV reconfigurable antenna is from 0V to 10 V which is lower than MEMS reconfigurable antenna.

CHAPTER VI

SUMMARY AND CONCLUSION

A novel printed antenna for reconfigurable applications is prepared in this thesis work. The FE BST thin-film varactor reconfigurable antenna has been demonstrated. This CPW bowtie antenna has a compact structure with the total size $6 \times 6\ mm^2$. The analyzer, that is used to measure the frequency and the return loss, is HP 8720B network analyzer, and the probe is CASCADE SP-ACP40-GSG-150-C. This antenna is integrated with a FE BST thin-film varactor which can shift the range of the resonant frequency by approximately 0.5 GHz. Furthermore, the frequency can shift back to high frequency by adjusting the voltage from 0V to 10V. In this experiment, the reconfigurable antenna will not work when multiple varactors are added. Even the CPW bowtie antenna only works when two varactors are skipped, the resonant frequency shifts perfectly. For the final results, the measurement results of the resonant frequencies are higher than the simulation results, but the return loss of the fabricated reconfigurable antenna is better than the simulated antenna. In the future work, the more varactors will still be added and fabricated, and the different types of antennas will be used with the varactors.

In this thesis, the BTFV reconfigurable antenna is compared with MEMS reconfigurable antenna, and there are several advantages of using BTFV reconfigurable antenna than the MEMS reconfigurable antenna. First, the size of BTFV reconfigurable antenna is smaller than MEMS reconfigurable antenna, and this advantage can save more space than MEMS reconfigurable antennas in applications. Second, the cost-manufacture of the BTFV reconfigurable antenna is lower than MEMS reconfigurable antenna. Third, MEMS Antenna has fatigue behavior. Unlike MEMS reconfigurable antenna, BTFV reconfigurable antenna does not have anything to go bad. Also, MEMS reconfigurable antennas have coupling effect because the MEMS reconfigurable antenna uses MEMS switches to connect or disconnect two pieces of metal. When these metals are close enough, they may have coupling effect even though the MEMS switch is off.

The BTFV reconfigurable antenna has the characteristics of small size, low cost, and long use life. The BTFV reconfigurable antenna has been proved and demonstrated that the resonant frequencies can be shifted. Therefore, the reconfigurable antenna was achieved.

BIBLIOGRAPHY

[1] Constantine A. Balanis, Modern antenna handbook, Wiley,2008

[2] Faruque Ahamed "Varactor based capacitive shunt switch using $BaSrTio_3$ (BST) Thin-films for microwave application applications", Ph.D. Dissertation. Dec. 2006. Print.

[3] Lei Zhou "RF MEMS DC contact switch for reconfigurable antennas", MS Thesis San Diego State University, 2006. Web. May 11th, 2011

[4] E. Brown, "RF-MEMS switches for reconfigurable integrated circuits", *IEEE Trans Microwave Theory Tech* 46 (11), 1868 1998.

[5] S. Kanagala, F. Ahamed, U. Nath, S. Wakade, and G. Subramanyam "Electrical Modeling of Ferroelectric Tunable Microwave Components and Circuits" *Ferroelectrics*, Volume 329, Issue 1, 2005.

[6] Thin-film ferroelectric materials and devices, Edited by R. Ramesh, Kluwer Academic, Norwell, MA, 1997.

[7] S. S. Gevorgian and E. L.Kollberg, "Do We Really Need Ferroelectrics in Paraelectric Phase Only in Electrically Controlled Microwave Devices?" *IEEE Trans. Microwave. Theory Techn.* **49**(11), 2117–2124 (2001).

[8] F. A. Miranda, G. Subramanyam, F. W. Van Keuls, R. R. Romanofsky, J. D. Warner, and C. H. Mueller, "Design and development of ferroelectric tunable microwave components for Ku- and K-band satellite communications systems," *IEEE Trans. Microwave Theory and Tech.* **48**(7), 1181–1189 (2000).

[9] R. R. Romanofsky, J. Bernhard, G.Washington, F.W.VanKeuls, F. A. Miranda, and C. L. Canedy, "A K-Band Linear Phased Array Antenna Based on Ba0.6Sr0.4TiO3 Thin Film Phase Shifters," *IEEE MTT International Microwave Symposium Digest* **2**, 1351–1354 (2000).

[10] G. Subramanyam, F. Van Keuls, F. A. Miranda, R. R. Romanofsky, C. Canedy, S. Aggarwal, T. Venkatesan, and R. Ramesh, "Performance of a K-Band Voltage-Controlled Lange Coupler Using a Ferroelectric Tunable Microstrip Configuration," *IEEE Microwave and Guided wave Letters,* **10**(4) (2000).

[11] R. R. Romanofsky, F. W. Van Keuls, and F. A. Miranda, "A cryogenic GaAs PHEMT/ferroelectric Ku-band tunable oscillator," *J. Phys. IV. France* **8**, 171–174 (1998).

[12] C. H. Mueller, and F. A. Miranda, "Tunable Dielectric Materials and Devices for Broadband wireless communications", in *Ferroelectric and Acoustic Devices*, Eds: D. Taylor and M. Francombe (Academic Press, 2000).

[13] A.K. Skrivervik, J.-F. Zurcher, O. Staub and J.R. Mosig, "PCS Antenna Design: The Challenge of Miniaturization," *IEEE Trans. Antennas Propag*., vol. 43, (4), pages 12-27, 2001.

[14] F. Namin, T.G. Spence, D.H. Werner and E. Semouchkina, "Broadband, Miniaturized Stacked-Patch Antennas for L-Band Operation Based on Magneto-Dielectric Substrates," *IEEE Trans. Antennas Propag.,* vol. 58, (9), pages 2817-2822, 2010.

[15] X.-Y. Zhang, P. Wang, S. Sheng, F. Xu, and C. K. Ong, "Ferroelectric $Ba_xSr_{1-x}TiO_3$ thin-film varactors with parallel plate and interdigital electrodes for microwave applications," *Journal of applied physics,* **104**, 124110 (2008).

[16] Andargachew Desta Alemayehu "Microwave frequency thin BST film based tunable shunt and series interdigital capacitor device design", MS Thesis The University of Dayton, 2011. Web. Sept. 11th, 2011

[17] A. Tombak, J.-P. Maria, F. T. Ayguavives, Z. Jin, G. T. Stauf, A. I. Kingon, and A. Mortazawi, "Voltage-Controlled RF Filters Employing Thin-Film Barium–Strontium–Titanate Tunable Capacitors," *IEEE Trans. Microwave. Theory Techn.,* **51**(2), 462-467 (2003).

[18] J. Nath, D. Ghosh, J.-P. Maria, A. I. Kingon, W. Fathelbab, P. D. Franzon, and M. B. Steer, "An Electronically Tunable Microstrip Bandpass Filter Using Thin-Film Barium–Strontium–Titanate (BST) Varactors," *IEEE Trans. Microwave. Theory .,* **53**(9), 2707-2712 (2005).

[19] C. M. Carlson, T. V. Rivkin, P. A. Parilla, J. D. Perkins, and D. S. Ginley, A. B. Kozyrev, V. N. Oshadchy, and A. S. Pavlov, "Large dielectric constant (ϵ/ϵ_o >600) $Ba_{0.4}Sr_{0.6}TiO_3$ thin films for high-performance microwave phase shifters," *Applied Physics Letters,* 76 (14) 2000.

[20] A. Kozyrev, A. Ivanov, V. Keis, M. Khazov, V. Osadchy, T. Samoilova, O. Soldatenkov, A. Pavlov, G. Koepf, C. Mueller, D. Galt, and T. Rivkin, "Ferroelectric films: Nonlinear properties and applications in microwave devices," in *IEEE MTT-S Int. Microwave Symp. Dig.*, vol. 2, pp. 985–988 1998.

[21] Mike Golio, The RF and microwave handbook, CPC press, 2001.

[22] M J Lancaster, J Powell and A Porch, "Thin-film ferroelectric microwave devices," Supercond. Sci. Tchnol. 11, pp. 1323-1334, 1998.

[23] Guru Subramanyam, Frederick W. Van Keuls and Felix A. Miranda, "A K-Band Frequency Agile Microstrip Bandpass Filter Using a Thin-Film HTS/Ferroelectric/ Dielectric Multilayer Configuration," IEEE Transaction on Microwave Theory and Techniques, vol. 48. 4, pp.525-530, April 2000.

[24] G. Subramanyam, F. Ahamed and R. Biggers, "A Si MMIC Compatible Ferroelectric Varactor Shunt Switch for Microwave Application," *IEEE Microwave and Guided Wave Lett.*, vol. 15, (11), pages 739-741, 2005.

[25] C.M. Bartsch, G. Subramanyam, J. Grote, F.K. Hopkins, L.L. Brott and R.R. Naik, "A New Capacitive Test Structure for Microwave Characterization of Biopolymers," *Microwave Opt. Tech. Lett.*, vol. 49, (6), pages 1261-1265, 2007.

[26] A. A. Eldek, A. Z. Elsherbeni, and C. E. Smith, "Characteristics of bow-tie slot antenna with tapered tuning stubs for wideband operation," *Progress In Electromagnetics Research* vol.49, pages 53-69, 2004.

[27] E.A. Soliman, S. Brebels, G.A.E. Vandenbosch and , E. Beyne, "Xband Brick Wall Antenna Fed by CPW," *Electron. Lett.,* vol. 34, (9), pages 836-838, 1998.

[28] M.-E. Chen and J.-H. Wang, "CPW-fed crescent patch antenna for UWB applications," Electron. Lett., vol. 44, (10), pages 613–614, 2008.

[29] H. Jiang, M. Patterson, C.H. Zhang and G. Subramanyam, "Frequency Agile Microstrip Patch Antenna Using Ferroelectric Thin Film Varactor Technology," *Proc. IEEE AP-S Int. Symp. Dig.*, pages 1-4, 2009.

[30] Lin, Y. D. and S.-N. Tsai, "Coplanar waveguide-fed uniplanar bow-tie antenna," *IEEE Trans. Ant. Prop.*, Vol. AP-45, No. 2, 305–306, Feb. 1997.

[31] Eldek, A. A., A. Z. Elsherbeni, C. E. Smith, and K-F Lee, "Wideband slot antennas for radar applications," *Proc. IEEE Radar Conf.,* 79–84, Huntsville, AL, May 2003.

[32] Soliman, E. A., S. Berbels, P. Delmotte, G. A. E. Vandenbosch, and E. Beyne, "Bow-tie slot antenna fed by CPW," *Electron Lett.,* Vol. 35, 514–515, 1999.

[33] Huang, J. F. and C.-W. Kuo, "CPW-fed bow-tie slot antenna," *Microwave Opt. Technol. Lett.*, Vol. 19, No. 5, 358–360, Dec. 1998.

[34] Miao, M., B. L. Ooi, and P. S. Kooi, "Broadband CPW-fed wide slot antenna," *Microwave Opt. Technol. Lett.*, Vol. 25, No. 3, 206–211, May 2000.

[35] Eldek, A. A., A. Z. Elsherbeni, and C. E. Smith, "Wideband bow-tie slot antennas for radar applications," *2003 IEEE Topical Conference on Wireless Communication Technology*, Honolulu, Hawaii, October 2003.

[36] E.A. Soliman, S. Brebels, P. Delmotte, G.A.E. Vandenbosch and E. Beyne, "Bow-tie slot antenna fed by CPW," *Electron. Lett.*, vol. 35, (7), pages 514-515, 1999.

[37] B. Riehl, G. Subramanyam, R. Biggers, A. Campbell, F.W. Van Keuls, F.A. Miranda and D. Tomlin, "Synthesis and characterization of nanostructured BSTO thin-films for microwave applications," *Integrated Ferroelectrics*, vol. 55, pages 825-837, 2003.

[38] A.L. Campbell, R.R. Biggers, G. Subramanyam, G. Kozlowski, R.A. Kleismit, H.N. Zate, S.C. Hopkins, B.A. Glowacki, B.D. Riehl, and T.L. Peterson, "Microwave characterization of nanostructured ferroelectric Ba0.6Sr0.4TiO3 thin films fabricated by pulsed laser deposition," *Nanotechnology*, vol. 19, (48), pages 485704.1-485704.14, 2008

[39] Richard L. Liboff and G. Conrad Dalman, "Transmission Lines waveguide and Smith Chart," Macmillan, New York, pp237-238.

[40] Fundamentals of microfabrication: the science of miniaturization, Edited by Marc J. Madou, CRC Press, 2002.

[41] Introduction to Microfabrication Edited by Sami Franssila, Wiley 2010

[42] Kagan Topalli, Emre Erdil, and Ozlem Aydin Civi, "Reconfigurable antenna structures using mems technology," web http://www.ursi.org/Proceedings/ProcGA05/pdf/B04P.20(0210).pdf, 2005.